Evaluation of Wind Tunnel and Scaling Effects with the UH-60A Airloads Rotor

Thomas R. Norman and Randall L. Peterson
National Aeronautics and Space Administration

Thomas H. Maier and Hyeonsoo Yeo
Aeroflightdynamics Directorate (AMRDEC)
U.S. Army Research, Development, and Engineering Command

ABSTRACT

Data obtained during the recently completed full-scale UH-60A Airloads wind tunnel test have been compared with measurements from the full-scale UH-60A Airloads flight test and the UH-60A small-scale test in the German-Dutch Wind Tunnel (DNW). Rotor power, airloads (section normal force and moment), and structural loads have been examined and compared to help understand the effects of the wind tunnel and model scale on the measured data. The measured power matched well with both flight and small-scale results, suggesting that the procedures and trim targets used to match the rotor conditions were fundamentally sound. For the flight test comparisons, rotor airloads were generally well simulated in the wind tunnel, although there were noticeable differences in the waveforms at the outboard radial stations that can't be explained by bad measurements or integration errors. Rotor structural loads were also well simulated with the exception of chord bending moments. Further investigation is necessary to determine the exact cause of these differences. For the DNW test comparisons, the rotor airloads and structural loads showed significant differences in waveform, especially for 3/rev torsion loads. These results are consistent with those found during earlier DNW/flight test comparisons and provide additional verification that the different blade modal properties of the DNW model had a significant effect on blade response and ultimately, blade airloads.

NOTATION

a_∞	free-stream speed of sound, ft/s
A	rotor disk area, πR^2, ft^2
c	section blade chord, ft
C_{CB}	chord bending coefficient, $M_{CB}/\rho\,(\Omega R)^2\,AR$
C_{DL}	damper load coefficient, $F_{DL}/\rho\,(\Omega R)^2\,A$
C_{FB}	flap bending coefficient, $M_{FB}/\rho\,(\Omega R)^2\,AR$
C_{Mx}	hub rolling moment coefficient, $M_x/\rho\,(\Omega R)^2\,AR$
C_{My}	hub pitching moment coefficient, $M_y/\rho\,(\Omega R)^2\,AR$
C_P	rotor power coefficient, $P/\rho\,(\Omega R)^3\,A$
C_{PL}	pitch link load coefficient, $F_{PL}/\rho\,(\Omega R)^2\,A$
C_Q	rotor torque coefficient, $Q/\rho\,(\Omega R)^2\,AR$
C_T	rotor thrust coefficient, $T/\rho\,(\Omega R)^2\,A$
C_{TO}	blade torsion coefficient, $M_{TO}/\rho\,(\Omega R)^2\,AR$
f_c	section force parallel to local chord, lbf/ft
f_n	section force perpendicular to local chord, lbf/ft
F_{DL}	damper load, lbf
F_{PL}	pitch link load, lbf
m	section moment about local ¼ chord, ft-lbf/ft
M	section Mach number
M^2c_m	section pitch moment coefficient, $m/(1/2\rho\,a_\infty^2c^2)$
M^2c_n	section normal force coefficient, $f_n/(1/2\rho\,a_\infty^2c)$
M^2C_p	blade pressure coefficient, $(p-p_\infty)/(1/2\rho\,a_\infty^2)$
M_{CB}	blade chord bending moment, ft-lbf
M_{FB}	blade flap bending moment, ft-lbf
M_{TO}	blade torsion moment, ft-lbf
M_{tip}	hover tip Mach number, $\Omega R/a_\infty$
M_x	rotor hub rolling moment, positive roll right, ft-lbf
M_y	rotor hub pitching moment, positive nose up, ft-lbf
p	blade surface pressure, lbf/ft^2
p_∞	free stream static pressure, lbf/ft^2
P	rotor power, ft-lbf/s
Q	rotor torque, ft-lbf
R	rotor radius, ft
T	rotor thrust, lbf
V_∞	free-stream velocity, ft/s
x	chordwise distance from leading edge, ft
α_c, α_s	corrected/geometric shaft angles, deg
β_{1c}, β_{1s}	cos/sin components of flapping, deg
μ	advance ratio, $V_\infty/\Omega R$
ψ	rotor azimuth angle, deg
ρ	free-stream density, $slugs/ft^3$
Ω	rotor angular rotation rate, rad/s
σ	rotor solidity

INTRODUCTION

A full-scale wind tunnel test of the UH-60A airloads rotor (Fig. 1) was recently completed in the National Full-Scale Aerodynamics Complex (NFAC) 40- by 80-Foot Wind Tunnel (Ref. 1). The rotor was the same one tested during the landmark 1993-94 NASA/Army UH-60A Airloads flight

Presented at the American Helicopter Society 68th Annual Forum, Fort Worth, Texas, May 1-3, 2011.

test (Fig. 2 and Refs. 2, 3) and included a highly pressure-instrumented blade to measure rotor airloads. In addition, the rotor was aerodynamically similar, with nearly identical instrumentation (including blade pressures), to the scaled rotor tested in the Large Low-speed Facility of the German-Dutch Wind Tunnels (DNW) in 1989 (Fig. 3, Refs. 4, 5).

One of the objectives of the NFAC test was to provide data to help evaluate the wind tunnel and scaling effects between small-scale wind tunnel, full-scale wind tunnel, and full-scale flight tests. To accomplish this, data were acquired at a limited number of conditions matching (to the greatest extent possible) those tested during the DNW and flight tests. The resultant three-test data set provides a unique evaluation opportunity similar to Refs. 6-7 and 8, with the added benefit of rotor airload measurements.

Prior to the NFAC test, efforts had been made to correlate the flight test data with DNW results (Refs. 2, 9). One of the primary issues in this correlation was that the flight test was conducted after the wind tunnel test, making the matching of conditions very difficult. This was made more difficult because of uncertainties in determining flight-test rotor thrust as well as differences in trim procedures for each test (minimized flapping for the DNW and propulsive/moment trim for flight). Ultimately, the flight/DNW comparisons of measured airloads showed clear differences at several radial stations and flight conditions. Further analysis (Ref. 10) suggested that these differences were likely caused by differences in the torsional response of the flight and DNW blades (caused by different blade modal properties). The current comparisons with the NFAC test provides the opportunity to re-investigate the scalability of the DNW rotor by eliminating the uncertainties associated with the trim conditions.

Three flight test and three DNW test conditions were matched during the NFAC test program. This paper will compare key measurements from these tests, including rotor power, integrated airloads, and structural loads, to help understand the effects of the wind tunnel walls and scaling.

DESCRIPTION OF EXPERIMENTS

The following section provides summaries of the test hardware, instrumentation, and data acquisition for each of the three airload tests. Particular emphasis is placed on information relevant to the comparisons between tests.

Flight Test

The Airloads flight test (Refs. 2, 3) used a UH-60A Blackhawk aircraft with an extensively instrumented rotor system. The four-bladed, articulated rotor system consisted of four subsystems: hub, blade pitch controls, bifilar vibration absorber, and main rotor blades. The four titanium-spar main rotor blades attached to spindles that were retained by elastomeric bearings to a one-piece titanium hub. These bearings permitted blade flap, lead-lag, and pitching motion.

Figure 1. UH-60A Airloads rotor installed in NFAC 40-by 80-Foot Wind Tunnel.

Figure 2. UH-60A Airloads rotor in flight.

Figure 3. UH-60A small-scale rotor installed in DNW.

Main rotor dampers were installed between each of the main rotor spindles and the hub to restrain lead-lag motion of the main rotor blades during rotation. A bifilar pendulum-type

vibration absorber system was mounted on top of the hub to reduce 3/rev rotating in-plane loads.

For the flight test, two of the rotor blades were heavily instrumented: one with 242 pressure transducers and one with a mix of strain-gages and accelerometers. 221 of the pressure transducers were installed in 9 chordwise arrays on the first blade and 21 strain gages (flap, chord, torsion) were installed on the second blade. Additional instrumentation included strain gages on the pitch links, dampers, and rotor shaft (for bending and torque). Angle of attack, sideslip, and airspeed were measured with instruments on the aircraft boom.

All pressure signals were filtered using 550 Hz low-pass 6-pole Butterworth filters and digitized at a rate of 2142 samples/sec/channel. The non-pressure signals were filtered using 110 Hz low-pass 6-pole Butterworth filters and digitized at a rate of 357 samples/sec/channel. For a typical level-flight test condition, a 5 second time slice (approximately 19 revolutions) was stored in the database.

NFAC Test

The NFAC test (Ref. 1) used the same four rotor blades flown during the Airloads flight test. The remaining rotor system hardware was predominantly UH-60A flight hardware (although not the same as used in flight), including spindles, hub, pitch links, and swashplate. For this test, the bifilar four-arm plate was installed but the pendulum weights were not attached (no 3/rev in-plane load absorption).

The rotor assembly was mounted on a large test stand with its own fixed system controls and rotor drive system (transmission, electric motors). The interface between the UH-60A rotor and test stand occurred at three locations: the UH-60A shaft extender and test stand shaft, the swashplate guide and transmission, and the non-rotating swashplate and the fixed system controls. The rotor and test stand was installed on a three-strut support system in the NFAC 40- by 80-Foot Wind Tunnel (Fig. 1).

The rotor blade instrumentation was essentially identical to the flight test, with five additional blade torsion gages installed on the strain-gage blade. Equivalent pitch link, damper, and shaft bending gages were also installed. The test stand included a rotor balance and flex-coupling to provide direct measurements of rotor hub forces/moments and shaft torque. Angle of attack was measured based on model rotation and airspeed based on calibration of wind tunnel wall pressures.

All pressure signals were filtered using 2000 Hz low-pass filters and digitized at a rate of 2048 samples/rev/channel. The non-pressure signals were filtered using 400 Hz filters and digitized at a rate of 256 samples/rev/channel. Corrections for the time delay caused by the anti-aliasing filters were incorporated in the data reduction process. A typical NFAC test point consisted of 128 revolutions of data.

DNW Test

The DNW test (Refs. 4, 5) used a 1/5.73-scaled pressure-instrumented model of the UH-60A main rotor. The scaled model blade geometry was identical to the full-scale blades except that it did not have trim tabs. Structural properties were similar to the full-scale blades with the exception of an increase in mass due to fabrication compromises necessary to install the pressure transducers. As a result, the DNW blades were dynamically scaled for only the first three modes. The resultant modal frequencies (Ref. 11) are compared with the full-scale rotor in Fig. 4 (Ref. 10).

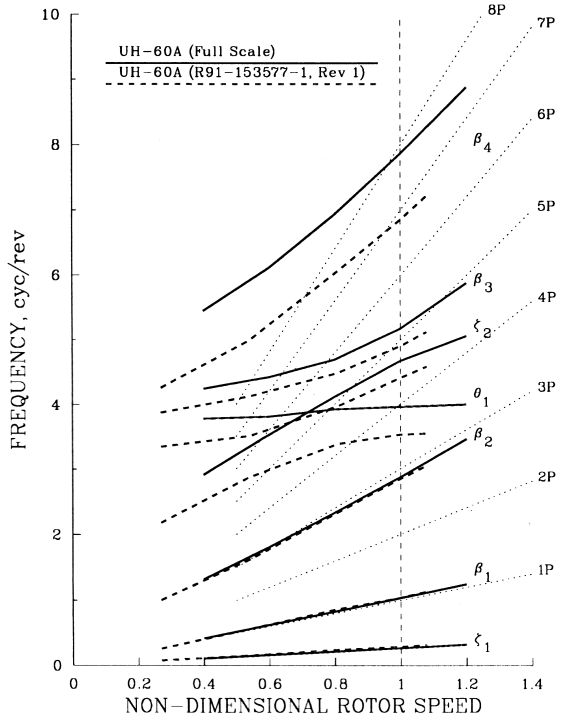

Figure 4. Calculated blade modal frequencies for full-scale and small-scale UH-60A rotors (from Ref. 10).

The blades were attached to a fully articulated hub with viscous lag dampers, which was mounted on a small-scale test stand with its own swashplate and fixed system controls. The hub and control system were not designed to match the full-scale flight vehicle (including no bifilar). The rotor and test stand were sting-mounted in the Large Low-speed (open-jet) Facility of the German-Dutch Wind Tunnels (DNW).

A total of 176 pressure transducers were installed in 10 chordwise arrays, 9 of which match the radial locations for the full-scale blade. The transducers were divided among the four blades to provide a more even mass distribution. Sixteen strain gages (flap, chord, torsion) were installed on one blade. The test stand included a rotor balance and flex-coupling to provide direct measurements of rotor hub

forces/moments and shaft torque. Angle of attack was measured based on model rotation and airspeed based on calibration of wind tunnel wall pressures.

All data signals were filtered using 10kHz low-pass 4-pole Butterworth filters and digitized at a rate of 1024 samples/rev/channel. A typical DNW test point consisted of 64 revolutions of data.

TEST DATA AND MATCHING CONDITIONS

This section describes the specific flight and DNW trim parameters that were matched during the NFAC test, the trim parameters with the highest uncertainties, and the wind tunnel procedures used. The final numerical trim values for each of the matched conditions are then provided.

Flight Test Matching

During the flight test, level-flight data were obtained at specified advance ratios for constant aircraft weight coefficients. The rotor RPM was held nominally constant, the cyclic controls were used to trim the aircraft flight path to straight and level, and the resultant flapping angles and shaft angle were not controlled. Relevant measured flight test parameters included aircraft weight, airspeed, hub moments (derived from the rotating shaft bending gage), rotor RPM, and aircraft angle of attack.

Based on these measurements (as well as those for the NFAC test), it was determined that the best flight/NFAC matching would come by reproducing the following key non-dimensional and geometric parameters in the wind tunnel: tip Mach number (M_{tip}), advance ratio (μ), corrected rotor shaft angle (α_C), rotor thrust (C_T/σ), and the fixed system hub moments (C_{My}/σ and C_{Mx}/σ) derived from an equivalent NFAC shaft bending gage.

Of these parameters, the one with the highest uncertainty from the flight test was rotor thrust. Because there was no direct measure of this parameter, it was instead determined by subtracting an estimate for non-rotor lift and fuel burn from the aircraft weight. The non-rotor lift included the effects of the fuselage, stabilator, and tail rotor and was estimated from calculations and small-scale wind tunnel results as described in Ref. 9.

The parameter with the highest uncertainty when set in the wind tunnel was the corrected rotor shaft angle. When testing in a wind tunnel, the wind tunnel walls (for closed test sections) or shear layer (for open test sections) alter the streamlines around the model and change the loads and effective angle of attack on the model. Corrections for these effects are necessary to best match free-flight conditions. For this test, a simple Glauert-type correction (Ref. 12) was used to estimate the change in angle of attack of the model due to the tunnel walls. The equation and NFAC-specific parameters used in this test are the same as those in Ref. 8.

To account for these and other uncertainties, the NFAC test plan called for setting baseline conditions to match the estimated flight test conditions and then acquiring additional wind tunnel data for derivative points around this baseline. These derivatives included changes in thrust, hub moments (pitch and roll), and shaft angle.

During testing, the standard procedure was to set the rotor RPM and tunnel speed to match the target M_{tip} and μ, and then adjust the shaft angle (α_S) so the wind tunnel wall corrected angle (α_C) matched the flight test. The rotor controls were then adjusted to match rotor thrust (C_T/σ), and fixed system hub moments. If necessary, the shaft angle was further adjusted to match α_C exactly. For derivative points, one parameter was changed at a time while all others were held constant. Following this procedure, trim conditions were typically matched within 0.5% of the pre-test targets.

Post-Test Corrections of Flight Trim Conditions

During post-test analysis of the data, it was determined that some of the original flight trim targets had been incorrectly specified. The differences came from two sources. The first was that the original targets were based on data from a single revolution of flight test data. During preparations for this paper, it was decided to instead use an ensemble average of the flight data (19 revs). This resulted in updated values for most trim parameters (less than 1% change). The second and most significant source was from the application of azimuthal corrections to the flight data. Since the target hub moments were determined from the sine and cosine components of the shaft bending gage measurement, any change to the azimuth reference directly affected these rotor trim values.

Three azimuthal corrections were applied to the flight data. The first correction was to shift all of the flight data by 7 deg to account for the difference in the definition of zero azimuth angle. For the NFAC test, the zero azimuth reference aligned the center of the rotor hub, the center of the elastomeric bearing, points on the blade quarter-chord, and the centerline of the LRTA fairing (Fig. 5). This was consistent with the reference used in the flight test when acquiring data, but 7 deg different from that used for the reduced data provided to analysts for comparisons (and used to set the NFAC trim conditions for this test). Reference 13 provides a detailed description of these two reference systems.

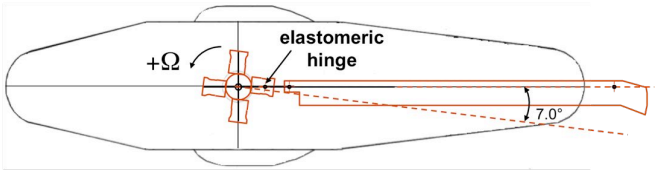

Figure 5. Definition of zero azimuth (and zero lag angle) for NFAC testing.

The second azimuthal correction was to shift all data for a given flight data point by the measured sideslip angle for that point. This correction aligns the zero azimuth reference of the rotor with the flight direction (rather than the fuselage) and is more consistent with the wind tunnel data (no sideslip/yaw). This correction is valid when comparing rotating measurements, but should be reassessed when looking at non-rotating measurements (i.e. fixed system control rod time histories).

The third azimuthal correction was to shift the flight data to correct for the signal delay caused by the flight test anti-aliasing filters (the NFAC data had already been corrected as described above). Assuming an ideal 110 Hz low-pass 6-pole Butterworth filter, the nominal group delay (time shift) of the signal as it goes through the filter is 0.00558 sec (group delays are actually slightly non-linear for this filter type). With the standard flight rotor speed of 258 RPM, this results in an azimuthal delay of approximately 8.6 deg. This azimuthal correction was applied to all the non-pressure channels from the flight test, including the shaft bending gage. For the 550 Hz filters used for the pressure channels, the equivalent delay is 0.00112 sec, resulting in a correction of 1.7 deg.

For comparisons with NFAC data, the flight test time history data was re-processed, including conversion from time-based to azimuthal data (256 samples/rev for pressure data, 64 samples/rev for non-pressure data), and all three azimuthal corrections noted above were applied. As would be expected, the rotor hub moments no longer exactly matched the trim targets used during the NFAC test.

DNW Test Matching

During the DNW test, simulated level-flight data were obtained at selected non-dimensional values of rotor lift and propulsive force for varying advance ratio. The lift and propulsive force were measured with the rotor balance, and collective and shaft angle were used to obtain the selected forces at each advance ratio. For all conditions, the cyclic controls were used to minimize the rotor first harmonic flapping.

After review of the available DNW data, it was determined that the best DNW/NFAC matching would come by reproducing the following key non-dimensional and geometric parameters in the wind tunnel: tip Mach number (M_{tip}), advance ratio (μ), corrected rotor shaft angle (α_c), rotor thrust (C_T/σ), and minimized first harmonic flapping. Thrust and shaft angle were chosen instead of lift and propulsive force to simplify matching the condition.

The parameter with the highest uncertainty for both wind tunnel tests was the corrected rotor shaft angle. As discussed above, wind tunnel corrections are necessary for both closed and open-jet test sections (the two corrections are in opposite directions). For the comparisons in this study, simple Glauert-type corrections were applied to both tunnels in a manner similar to Ref. 8.

During testing, the standard procedure was to set the rotor RPM and tunnel speed to match the target M_{tip} and μ, and the shaft angle (α_S) set so the wind tunnel wall corrected angle (α_c) matched the DNW test. The rotor controls were then adjusted to match the appropriate rotor thrust (C_T/σ) and minimize 1/rev flapping (from the root flap angle measurement on the pressure blade). If necessary, the shaft angle was further adjusted to match α_c exactly. Similar to the flight test comparisons, both baseline and derivative data points (varying thrust, shaft angle, and longitudinal flapping) were acquired. For derivative points, one parameter was changed at a time while all others were held constant. Following this procedure, trim conditions were typically matched within 0.5% of the pre-test targets.

No corrections to the DNW data were necessary in order to match with NFAC data. In particular, the DNW zero azimuth reference was similar to the NFAC (0 deg when center of hub, hinge point, and blade quarter-chord were aligned with the model tail), and the signal delays due to anti-aliasing filters were small (less than 0.4 deg for the 10 kHz filters).

Matched Data Points

Three flight test points and three DNW test points were simulated during NFAC testing following the procedures outlined above. These simulations included acquisition of data at the targeted trim conditions (identified as the NFAC baseline data points) as well as at the derivative conditions (for 5 of the 6 simulated conditions). Tables 1 and 2 list the relevant NFAC data points and measured trim values for the flight and DNW matched conditions (including one representative baseline data point and the average of all baseline points acquired). The trim values provided represent ensemble-averaged data for each test point (19 revs for flight, 64 revs for DNW, 128 revs for NFAC).

In Tables 1-2 and in the following sections, the flight, DNW, and NFAC test points are identified by their standard nomenclature from the literature. Examples include c8424 for flight (Flight counter 84, data point 24), 13.20 for the DNW (Run 13, data point 20), and R47P21 for the NFAC (Run 47, data point 21).

Because of the post-test corrections to the data described earlier, the baseline NFAC data points do not exactly match the trim conditions from flight and the DNW. Nevertheless, the trim values remained relatively close and are well within the trim range from the derivative points. It will be demonstrated later that the effects of these trim differences are small for the comparisons made in this paper.

It should also be noted that the matched conditions fall within a fairly narrow speed and thrust range (with the

exception of one high thrust case). Therefore it will not be possible to develop general scaling laws or make general assessments covering the entire flight regime. Nonetheless, the test comparisons should provide valuable insight into the effects of model scale and wind tunnel.

COMPARISON PARAMETERS

In the following sections, the rotor performance, blade airloads (section loads and pressures), and structural loads will be compared to identify the similarities and differences between tests. Non-dimensional values are used for comparison to account for differences in scale and atmospheric conditions.

It is noted that great care should be taken in the comparisons of sectional airloads, especially pitch moment. For these three tests, the rotor sectional airloads are calculated by integrating the measured pressures at a given radial station to provide normal force and pitch moment. The accuracy of the integrations is dependent on the number and validity of the pressure measurements used in the integration. Transducer failures or voltage offsets can significantly affect the calculated loads. This is especially true for the relatively small pitch moments in attached flow, where the high

Table 1. Flight/NFAC Matched Conditions

Pt Type	Pt #	M_{tip}	μ	α_c	C_T/σ	C_{My}/σ C_{Mx}/σ
Flight	**c8424**	**0.637**	**0.304**	**-4.32**	**0.088**	**-0.00092** **-0.00058**
Baseline	R47P21	0.637	0.303	-4.16	0.087	-0.00071 -0.00083
Avg BL	10 pts	0.638	0.304	-4.16	0.087	-0.00071 -0.00083
Pitch +	R47P16	0.638	0.304	-4.16	0.087	-0.00041 -0.00083
Pitch -	R47P17	0.638	0.304	-4.16	0.087	-0.00101 -0.00083
Roll +	R47P19	0.637	0.304	-4.16	0.087	-0.00071 -0.00052
Roll -	R47P20	0.637	0.304	-4.16	0.087	-0.00071 -0.00113
Thrust +	R47P22	0.637	0.304	-4.12	0.092	-0.00071 -0.00083
Thrust -	R47P23	0.637	0.304	-4.20	0.082	-0.00071 -0.00083
Alpha +	R47P25	0.637	0.303	-3.16	0.087	-0.00071 -0.00083
Alpha -	R47P26	0.638	0.303	-5.15	0.087	-0.00071 -0.00083
Flight	**c8525**	**0.642**	**0.233**	**-1.56**	**0.077**	**-0.00116** **-0.00022**
Baseline	R60P18	0.642	0.232	-1.48	0.077	-0.00119 -0.00036
Avg BL	6 pts	0.643	0.232	-1.48	0.077	-0.00119 -0.00036
Pitch +	R60P13	0.643	0.232	-1.48	0.077	-0.00088 -0.00036
Pitch -	R60P14	0.643	0.231	-1.48	0.077	-0.00149 -0.00036
Roll +	R60P16	0.643	0.231	-1.48	0.077	-0.00119 -0.00005
Roll -	R60P17	0.643	0.232	-1.48	0.077	-0.00119 -0.00066
Thrust +	R60P20	0.643	0.232	-1.42	0.082	-0.00119 -0.00036
Thrust -	R60P21	0.643	0.231	-1.54	0.072	-0.00119 -0.00036
Alpha +	R60P23	0.643	0.232	-0.48	0.077	-0.00119 -0.00036
Alpha -	R60P24	0.642	0.232	-2.49	0.077	-0.00119 -0.00036
Flight	**c9020**	**0.670**	**0.244**	**-0.52**	**0.118**	**-0.00059** **-0.00012**
Baseline	R60P28	0.669	0.245	-0.50	0.118	-0.00059 -0.00016
Avg BL	2pts	0.668	0.245	-0.50	0.118	-0.00059 -0.00016

Table 2. DNW/NFAC Matched Conditions

Pt Type	Pt #	M_{tip}	μ	α_c	C_T/σ	β_{1c} β_{1s}
DNW	**13.20**	**0.629**	**0.301**	**-3.76**	**0.098**	**-** **-**
Baseline	R47P40	0.629	0.300	-3.72	0.100	0.01 0.00
Avg BL	9 pts	0.628	0.300	-3.72	0.100	0.00 0.00
Flap +	R47P38	0.628	0.300	-3.72	0.100	0.50 -0.01
Flap -	R47P39	0.628	0.300	-3.72	0.100	-0.50 0.01
Thrust +	R47P41	0.629	0.299	-3.68	0.105	-0.01 0.00
Thrust -	R47P42	0.629	0.299	-3.75	0.095	0.00 0.00
Alpha +	R47P44	0.628	0.299	-2.72	0.100	-0.01 0.00
Alpha -	R47P47	0.628	0.300	-4.72	0.100	0.00 0.00
DNW	**11.24**	**0.637**	**0.152**	**6.85**	**0.070**	**-** **-**
Baseline	R67P42	0.637	0.152	6.94	0.071	0.00 0.00
Avg BL	8 pts	0.637	0.152	6.92	0.071	0.00 0.00
Flap +	R67P40	0.637	0.152	6.94	0.071	0.50 -0.01
Flap -	R67P41	0.637	0.151	6.95	0.071	-0.50 0.01
Thrust +	R67P43	0.637	0.151	7.10	0.076	0.00 0.00
Thrust -	R67P44	0.637	0.152	6.78	0.066	0.00 0.00
Alpha -	R67P46	0.637	0.152	5.93	0.071	0.00 0.00
DNW	**13.12**	**0.638**	**0.300**	**-0.04**	**0.070**	**-** **-**
Baseline	R67P22	0.638	0.300	-0.05	0.070	0.01 0.00
Avg BL	10 pts	0.638	0.300	-0.05	0.070	0.00 0.00
Flap +	R67P20	0.638	0.300	-0.05	0.070	0.50 -0.01
Flap -	R67P21	0.638	0.299	-0.05	0.070	-0.51 0.01
Thrust +	R67P23	0.638	0.300	-0.01	0.075	0.00 0.00
Thrust -	R67P24	0.638	0.299	-0.09	0.065	0.00 0.00
Alpha +	R67P26	0.638	0.300	0.95	0.070	0.00 0.00
Alpha -	R67P30	0.638	0.300	-1.05	0.070	0.00 0.00

leading edge suction balances the large trailing edge moment arms, resulting in the difference of two large numbers. In this case, small changes in the steady pressure measurements (due to drift, etc.) can have a large influence on the integrated moment. Although failed/failing transducers were removed from the integrations when found, it is possible that some less than perfect measurements remain in the integration. Any conclusions must account for this possibility.

RESULTS

This section provides the detailed NFAC comparisons with matched data points from flight and the DNW. In particular, comparisons of rotor power, airloads, and structural loads are made. All available matched conditions are used for power comparisons, while the airload and structural load comparisons focus mainly on the higher thrust points at μ=0.30 (c8424, 13.20).

Flight Test Simulation

Power

Figure 6 shows a comparison of non-dimensional rotor power (C_P/σ) for the three flight test conditions (c8424, c8525, c9020). For each condition, the flight test power is compared to one representative NFAC baseline point, the average from all NFAC baseline points, and the average corrected power from all NFAC points. The corrected values were determined using the derivative data acquired during testing to determine the sensitivity of rotor power to each change. These linear slopes were then used to correct the measured power, assuming linear superposition of all effects. No corrected values are provided for c9020 since no derivative data were acquired for this condition.

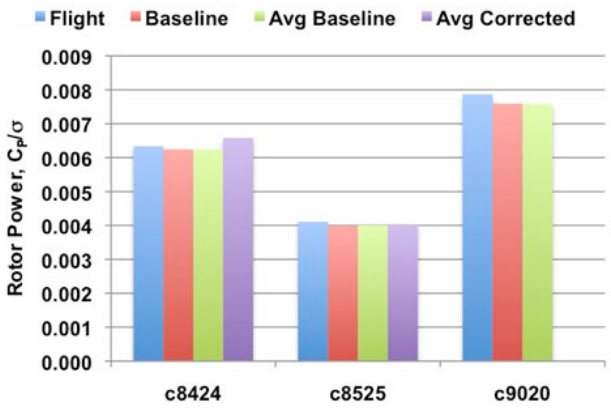

Figure 6. Comparison of NFAC rotor power with flight test for three forward flight conditions.

The effects of trim changes on rotor power are shown for one simulated flight condition (c8424) in Fig. 7. These data show that hub pitching moment, thrust, and shaft angle all have significant effects on power while rolling moment does not. This was expected as each of these trim parameters directly affects the rotor propulsive force.

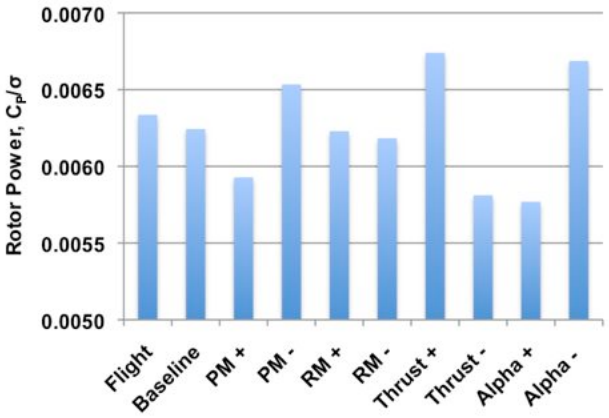

Figure 7. Effect of NFAC trim target derivatives on rotor power for one forward flight condition (c8424 simulation).

For the c8424 comparison, the NFAC baseline and averaged baseline power are reasonably close to the flight test power (1.5% low, $\Delta C_P/\sigma$=-0.0001) even though the trim conditions were not matched exactly. After correction, the NFAC power is 3.5% higher ($\Delta C_P/\sigma$=+0.0002). For c8525 and c9020, the baseline trim conditions matched the flight data more closely, and the baseline power was 2.5% and 3.5% lower, respectively ($\Delta C_P/\sigma$=-0.0001 and -0.0003). Corrections for c8525 had a negligible effect.

For this limited number of flight test conditions, the corrected NFAC power is slightly higher for one case and lower for the other two. This makes it difficult to attribute the differences to a single systematic error (i.e. the flight test thrust is always high, or the wall corrected shaft angle is always low). Nevertheless, the consistency (and small differences) between the power measurements suggests that the flight test matching procedure was sound.

Airloads

The rotor airloads are investigated in this section, with the primary emphasis on the c8424 condition. For these comparisons, data from the NFAC baseline condition (R47P21) were used.

Figure 8 shows the normal force distribution along the blade and around the azimuth for the c8424 flight test condition. This radial contour plot shows many of the features expected in high-speed forward flight, including negative lift near the tip in the second quadrant to accommodate roll moment balance (and other effects) as well as negative lift on the inboard sections of the retreating blade due to reverse flow. The lift distribution varies around the azimuth with the highest lift near the forward and aft sections of the rotor.

Figure 9 shows the difference in normal force distribution between the flight test and the NFAC test. This figure

suggests that there were no major normal force differences on the inboard portion of the blade. There were differences on the outboard portion of the blade, however, with the NFAC test providing less lift on the retreating side and more in the negative lift portion of the second quadrant. More detailed comparisons are provided in Figs. 10-13.

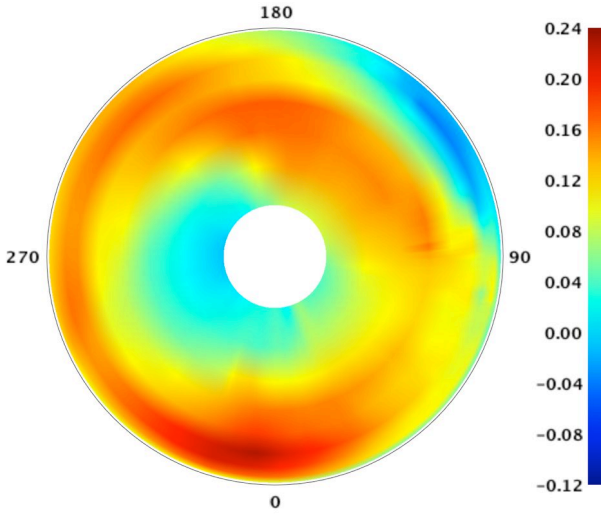

Figure 8. Section normal force distribution (M^2c_n) for flight test condition (c8424).

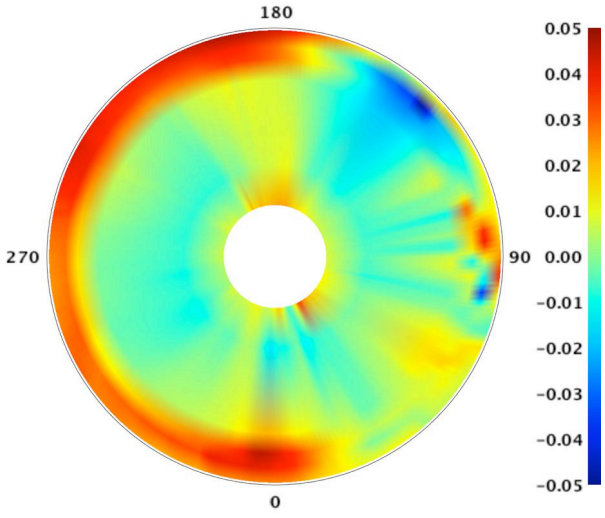

Figure 9. Difference in section normal force distribution (M^2c_n) between flight test (c8424) and NFAC (R47P21).

Figures 10 and 11 show the non-dimensional normal force and pitch moment for r/R=0.225, 0.40, and 0.775. There is generally good agreement at these radial stations. The normal force shape and magnitudes match well, with slightly higher force levels indicated in flight test at r/R=0.225. The pitch moment shapes also match well but there are significant magnitude offsets at r/R=0.225 and 0.40. These offsets are caused by steady pressure offsets in some of the trailing edge transducers, as discussed earlier.

Figures 12 and 13 show the normal force and pitch moment for r/R=0.865, 0.92, and 0.99. The normal force comparisons are consistent with the qualitative results from Fig. 9, where the NFAC data shows less lift on the retreating side of the rotor and more in the negative lift section of the second quadrant. Also of note is the reduced rate of change of NFAC normal force between ψ=120 and 240 deg at these outboard stations. The pitch moments (Fig. 13) also show noticeable differences, especially at r/R=0.865 and 0.92. For these radial stations, the NFAC data show more negative moment on the advancing side and an increased rate of change between ψ=120 and 240 deg. The NFAC data does replicate most of the aerodynamic features seen in the flight test data, however, including the shock- and vortex-induced loading near ψ=90 deg.

The airload data were investigated further to help determine whether the noted differences might be due to either 1) incorrect trim conditions or 2) the quality and/or number of working pressure transducers used in the integrations. The sensitivity of the results to trim conditions can be seen in Figs. 14 and 15 for r/R=0.92. For normal force (Fig. 14), changes in hub pitching moment, shaft angle, and rolling moment (not shown) had minimal effect. Changes due to rotor thrust (Fig. 14a) are noticeable. However, the thrust variations result in predominantly a mean shift of the normal force, with minimal differences in the waveform.

Figure 15 shows the effects of trim changes on section pitch moment. For this case, only increased hub pitching moment showed any effect on the section loads. This was perplexing, since the equivalent decrease in hub pitching moment had no effect. Further investigation found that for the increased hub pitching moment case (R47P16), one additional transducer had been used in the integration (x/c=0.164 on the lower surface). If this transducer is removed, then the trim variation does not show any impact on the section pitch moment. This highlights the sensitivity of the section pitch moment to the transducers used in the integration. In this case, the extra transducer is located near the shock on the lower surface (Fig. 16) and averaging around the missing transducer can provide significantly different results.

The data of Figs. 14 and 15 suggest that trim target errors are unlikely to be the cause of the differences between NFAC and flight airloads (similar results were found for other radial stations). To ensure that these differences are not caused by differences in the number of transducers used in the integrations, the flight and NFAC data at r/R=0.92 were recomputed using exactly the same transducer locations. This required eliminating two additional transducers from each integration. The resulting normal force and pitch

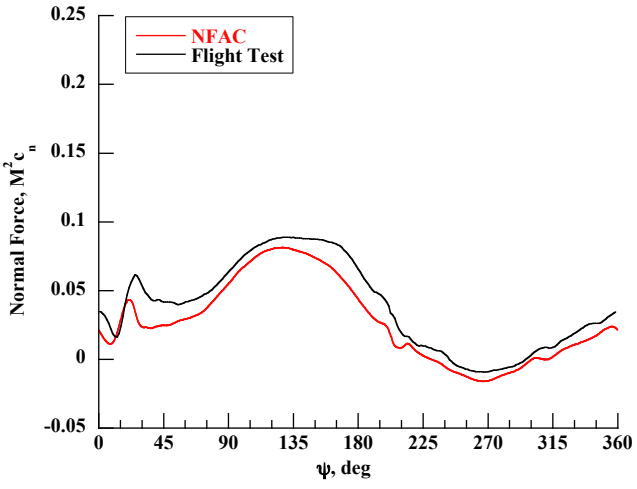

a) r/R=0.225

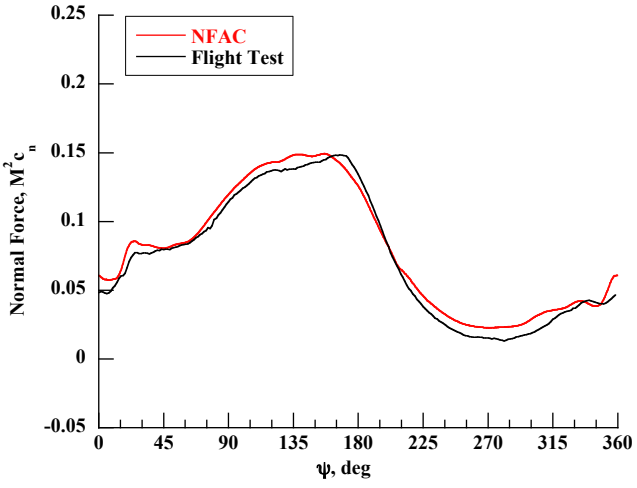

b) r/R=0.40

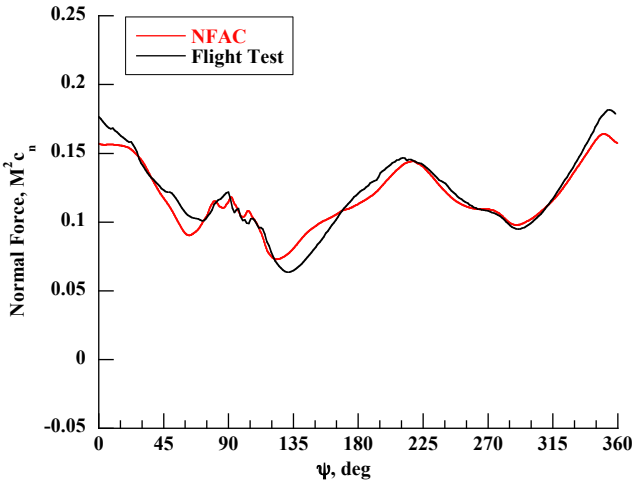

c) r/R=0.775

Figure 10. Comparison of NFAC section normal force (M^2c_n) with flight test (c8424, R47P21), r/R=0.225, 0.400, 0.775.

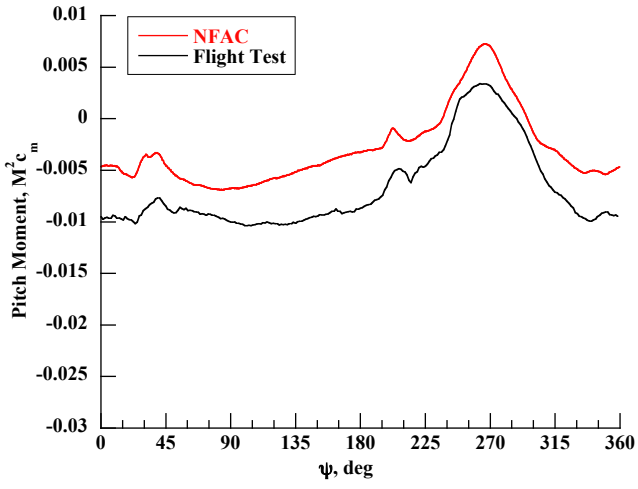

a) r/R=0.225

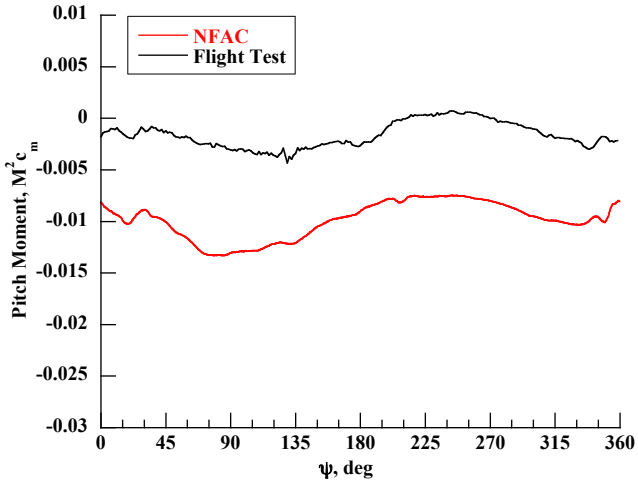

b) r/R=0.40

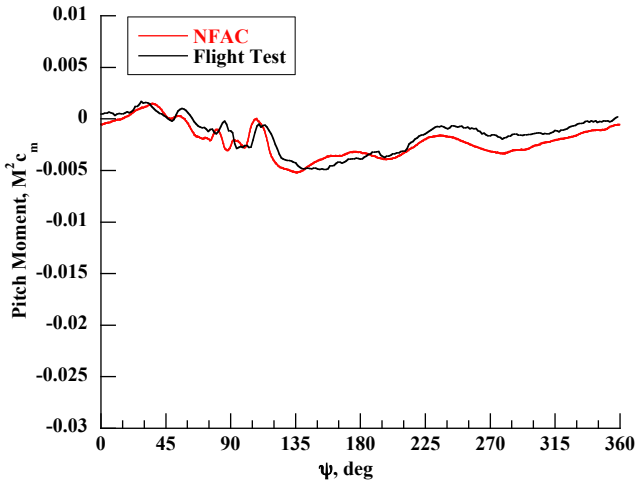

c) r/R=0.775

Figure 11. Comparison of NFAC section pitch moment (M^2c_m) with flight test (c8424, R47P21), r/R=0.225, 0.400, 0.775.

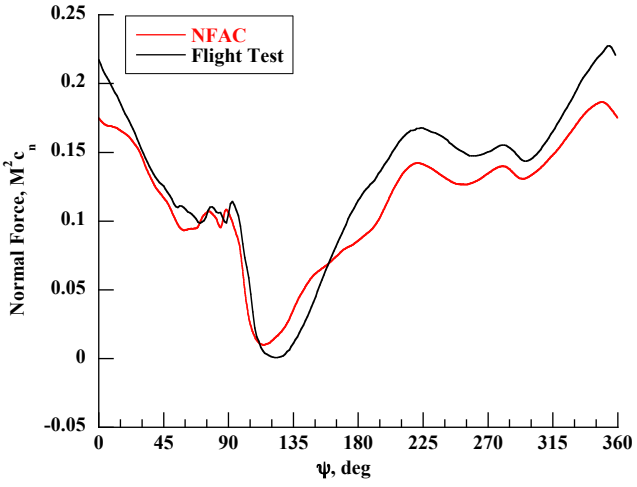

a) r/R=0.865

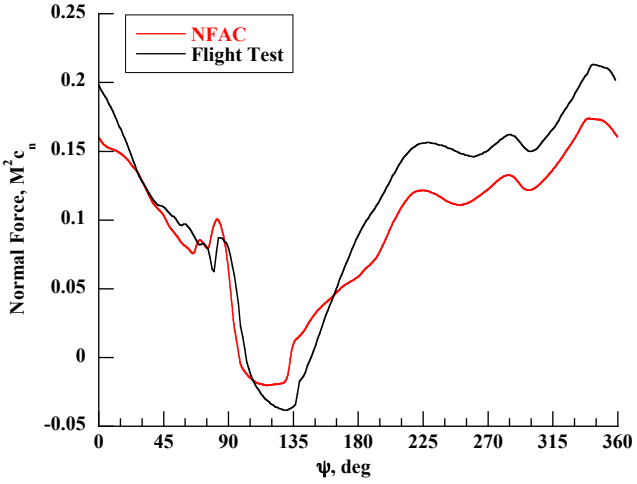

b) r/R=0.92

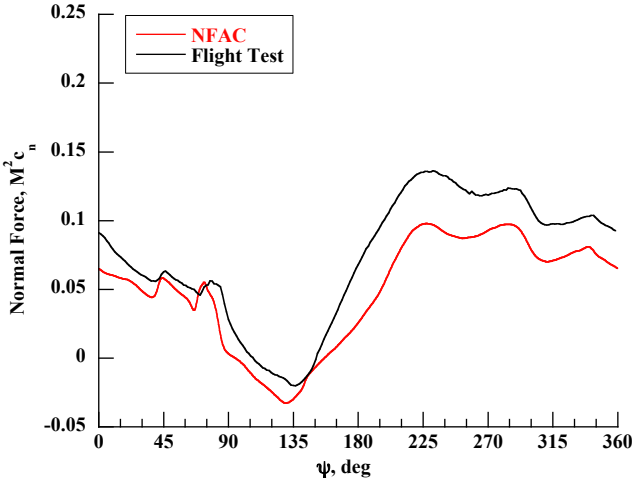

c) r/R=0.99

Figure 12. Comparison of NFAC section normal force (M^2c_n) with flight test (c8424, R47P21), r/R=0.865, 0.920, 0.990.

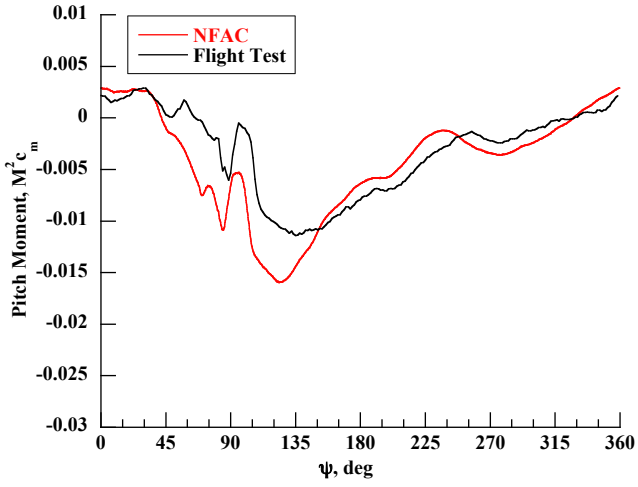

a) r/R=0.865

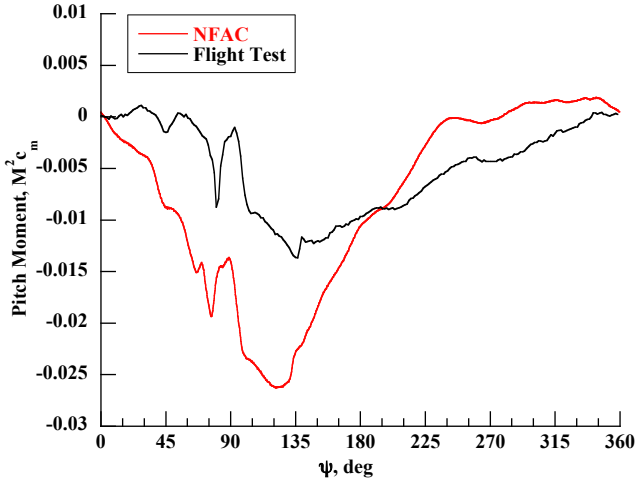

b) r/R=0.92

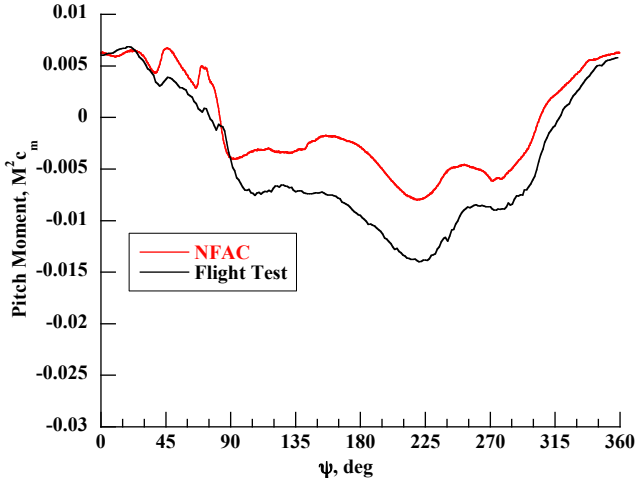

c) r/R=0.99

Figure 13. Comparison of NFAC section pitch moment (M^2c_m) with flight test (c8424, R47P21), r/R=0.865, 0.920, 0.990.

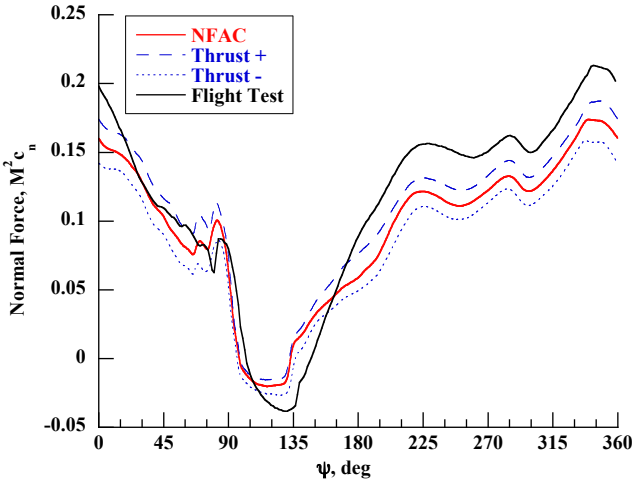

a) Thrust

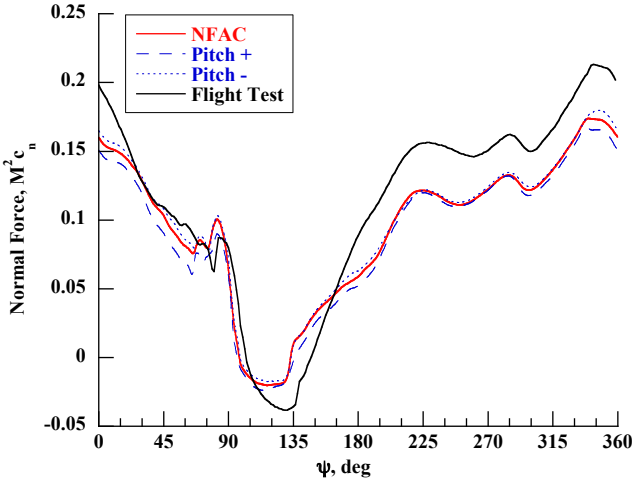

b) Hub Pitching Moment

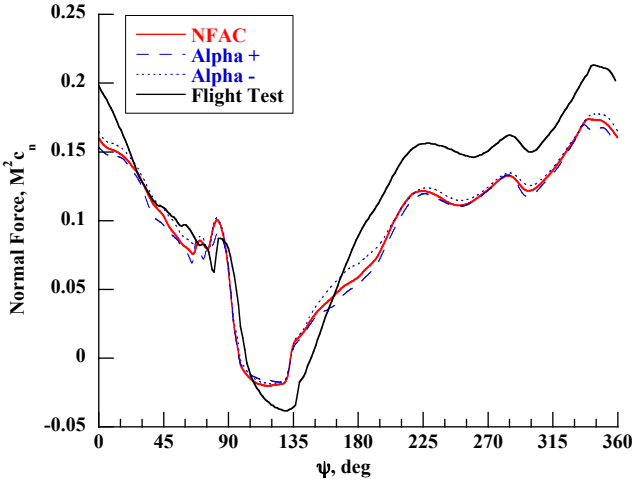

c) Shaft Angle

Figure 14. Effect of NFAC trim target derivatives on section normal force (M^2c_n), c8424 simulation, r/R=0.92.

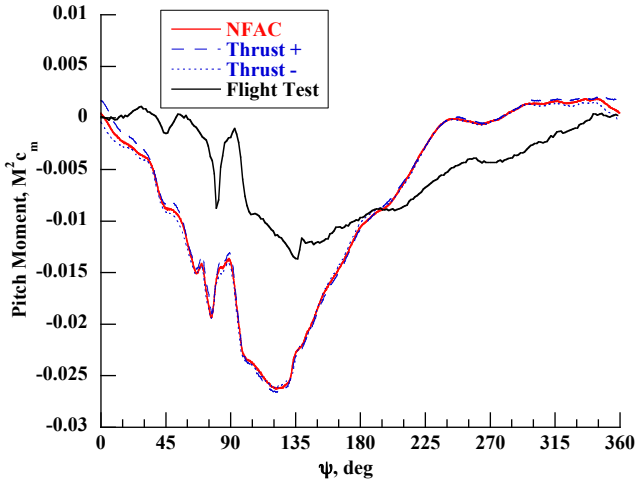

a) Thrust

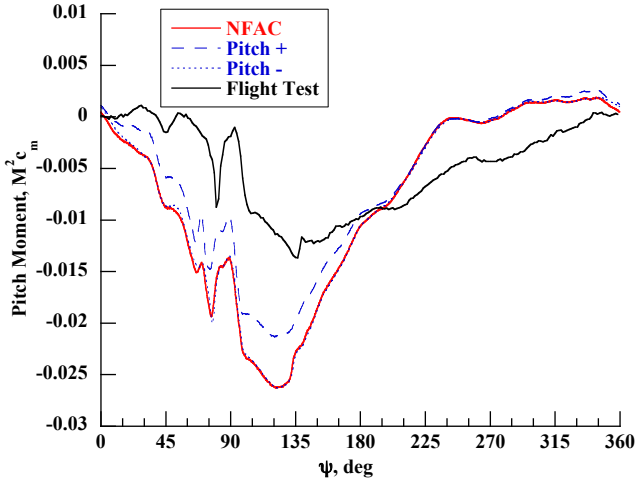

b) Hub Pitching Moment

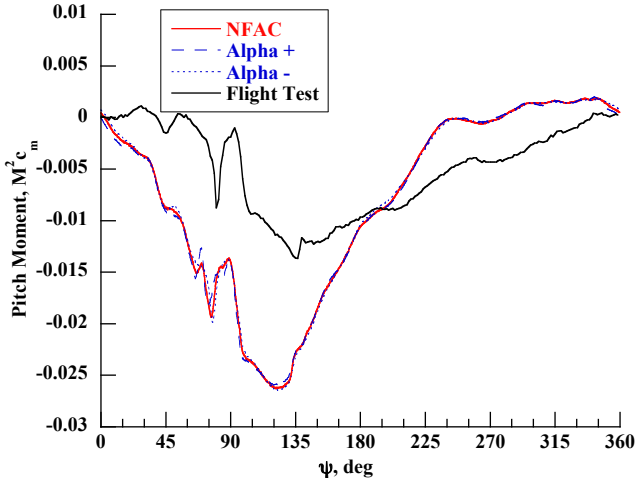

c) Shaft Angle

Figure 15. Effect of NFAC trim target derivatives on section pitch moment (M^2c_m), c8424 simulation, r/R=0.92.

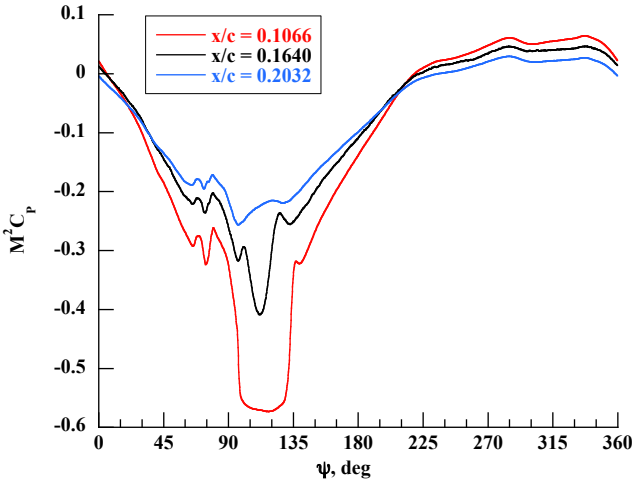

Figure 16. NFAC lower surface pressures near shock, r/R=0.92, (R47P16).

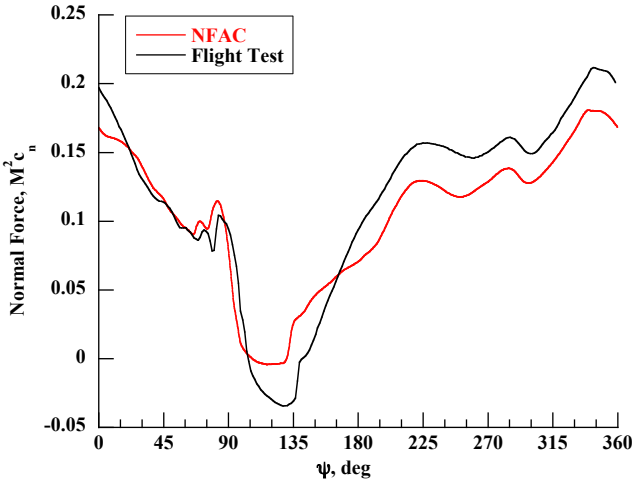

a) M^2c_n

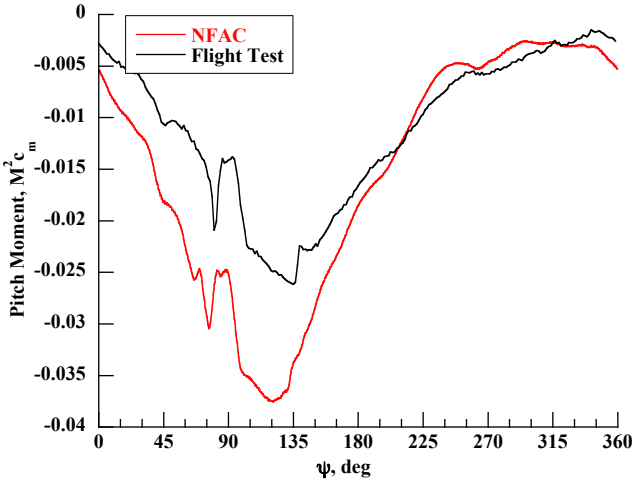

b) M^2c_m

Figure 17. Section normal force and pitch moment when using identical transducers in integration, r/R=0.92, (c8424, R47P21).

moments are shown in Fig. 17. Although the absolute magnitudes are changed from Figs. 12b and 13b (due to the reduced number of transducers), the relative differences in shape remain. Thus the differences do not appear to be caused by the number of transducers used in the integration.

Individual pressure measurements were then investigated to help understand the airload differences. Figure 18 shows the normalized pressures versus chordwise station (x/c) for four different azimuth locations at r/R=0.92. At ψ=0 (Fig. 18a), the flight test data show a consistently higher pressure differential across the entire airfoil when compared to NFAC data. This results in an increased flight test normal force and nominally equivalent moments (compare with Figs. 12b and 13b). At ψ=56.25 deg (Fig. 18b), the flight test pressure differential remains larger on the forward portion of the airfoil but has been significantly reduced on the aft portion (x/c>0.40). This results in equivalent normal force and a more positive moment from flight. At ψ=130.78 deg (Fig. 18c), the flight test pressure differential is now essentially equivalent to the wind tunnel on the forward portion, but the wind tunnel differential is now much greater than flight all along the aft portion. This results in a more negative flight test normal force and significantly less moment. Finally, at ψ=240.47 deg (Fig. 18d), the flight test pressure differential is once again consistently higher across the entire airfoil, with slightly higher differentials along the aft portion (compared to Fig. 18a). This results in more positive flight test lift and a slightly more negative moment.

The variations of pressures around the azimuth (shown in Fig. 18) suggest that the differences in integrated airloads for this radial station are not due to differences in a single transducer, but rather due to differences in whole groups of transducers. Thus, it appears that the airload differences at the outboard radial stations (Figs. 12 and 13) are real. The physical cause of these differences is not currently known. The proximity of the wind tunnel walls to the rotor during testing is the most likely cause, but differences in turbulence levels or aero/structure coupling could also be contributing factors. It is recommended that these differences be investigated computationally, comparing results both with and without the wind tunnel modeled to help isolate potential causes.

Airloads for the other two matched flight conditions are shown in Figs. 19-22 at three radial stations. The general trends for the c8525 case (Figs. 19 and 20) are similar to those shown for c8424. These include good correlation at the inboard stations, and noticeable differences at the outer stations. Similar trends can also be seen when looking at the pressure distributions (not shown).

The c9020 comparisons are shown in Figs. 21 and 22. The correlation with flight test is not as good for this high thrust condition. In addition to moment offsets at r/R=0.225 and 0.865, the NFAC data show normal force and moment shape differences, especially on the retreating side. Although the azimuthal location for the lift and moment stall events are

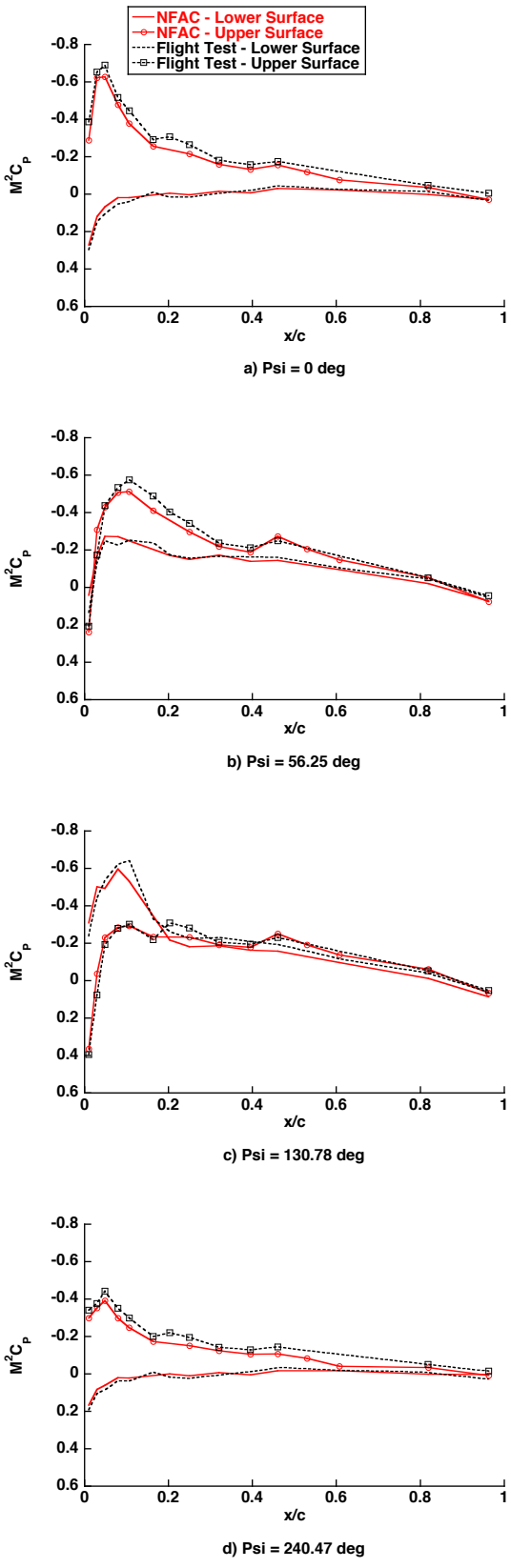

Figure 18. Chordwise pressure distributions at 4 azimuthal locations, r/R=0.92, (c8424, R47P21).

similar between tests, the relative magnitudes of the airloads at these events are different. The exact cause of these differences is not known. Although no derivative data were acquired in the wind tunnel for this flight test condition, it is known (Ref. 1) that the airloads are highly sensitive to trim conditions (especially thrust/collective) near the thrust limit for this rotor. Thus, the major differences seen in Figs. 21 and 22 could be caused by incorrect trim conditions.

Structural Loads

The rotor structural loads are investigated in this section, with the primary emphasis on the c8424 condition. For these comparisons, data from the NFAC baseline condition (R47P21) were used.

Comparisons of structural load time histories (with means removed) for the c8424 test condition are provided in Figs. 23 and 24. Blade bending moments are shown in Fig. 23 for representative radial stations. The normalized flap bending moment at r/R=0.60 (Fig. 23a) matches very well with flight test. The torsion moment at r/R=0.30 (Fig. 23b) also matches well (but not as well as flap bending), with the NFAC data showing some higher frequency content. The chord bending moment at r/R=0.60 (Fig. 23c) is similar in character to flight, but does not match nearly as well as the flap and torsion moments. In particular, the NFAC data shows lower amplitudes as well as some phase differences. Pitch link load, damper force, and rotor torque are compared in Fig. 24. These parameters also match well with slightly higher magnitudes in flight.

Comparisons of the blade bending loads for the other two matched flight conditions are shown in Figs. 25 and 26. The c8525 comparisons (Fig. 25) show results similar to the c8424 comparisons, with good matches for flap bending and torsion and less good for chord bending. For the c9020 comparisons (Fig. 26), neither the flap bending nor the torsion match as well as the other two cases (the chord bending gages were not operational during the flight test).

Further data analysis was performed on the best (flap bending) and worst (chord bending) matched data from the c8424 comparisons. Similar to the airload evaluation above, the effect of trim condition was evaluated on all gages. Sample results are provided in Figs. 27 and 28 for measurements at one radial station (r/R=0.60). For each, the effects of changes in thrust, hub pitching moment, and shaft angle are shown (rolling moment variations had minimal effect). None of the trim changes had a large effect on flap bending (Fig. 27), although the shaft angle change had the biggest effect. For chord bending, the trim changes were more noticeable, especially the thrust and shaft angle changes. The actual differences remained small, however, and the characteristic shapes of the time histories were not altered. These results are representative of other blade radial stations and other structural parameters and suggest that, similar to the blade airload results, trim target errors are

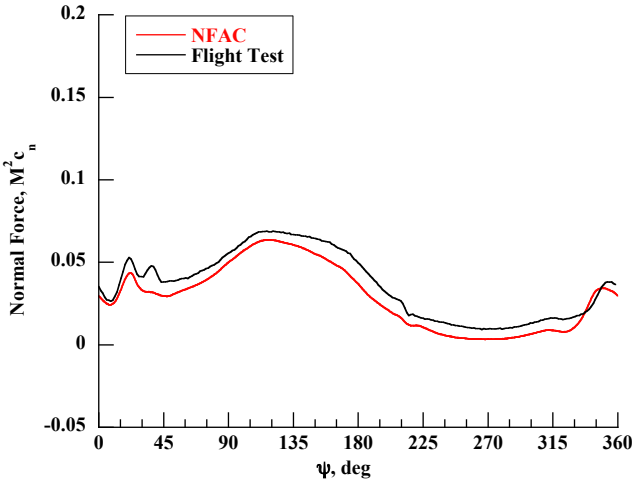

a) r/R=0.225

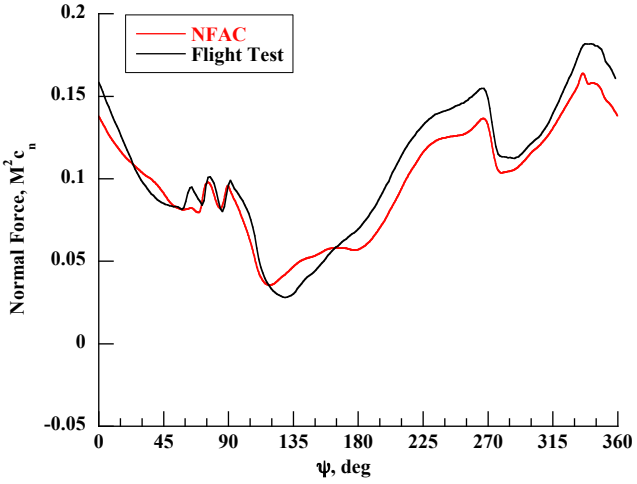

b) r/R=0.865

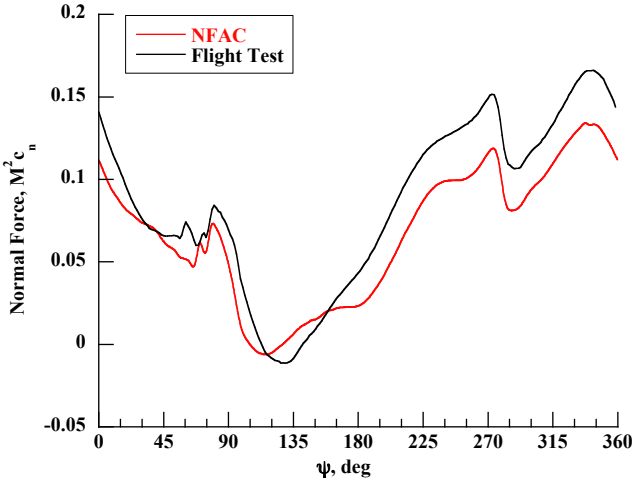

c) r/R=0.92

Figure 19. Comparison of NFAC section normal force (M^2c_n) with flight test (c8525, R60P18), r/R=0.225, 0.865, 0.920.

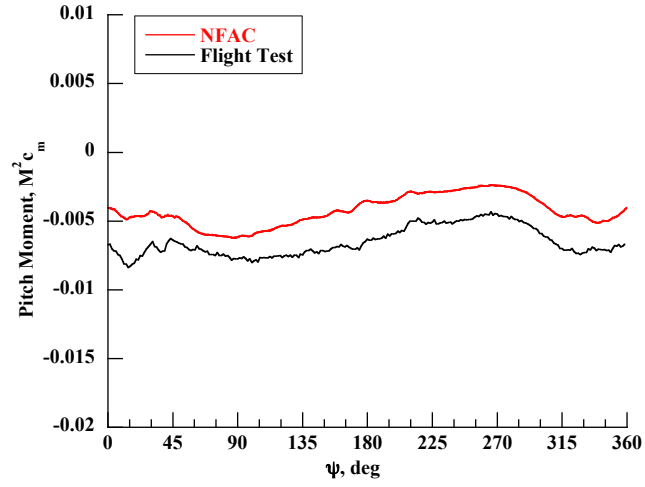

a) r/R=0.225

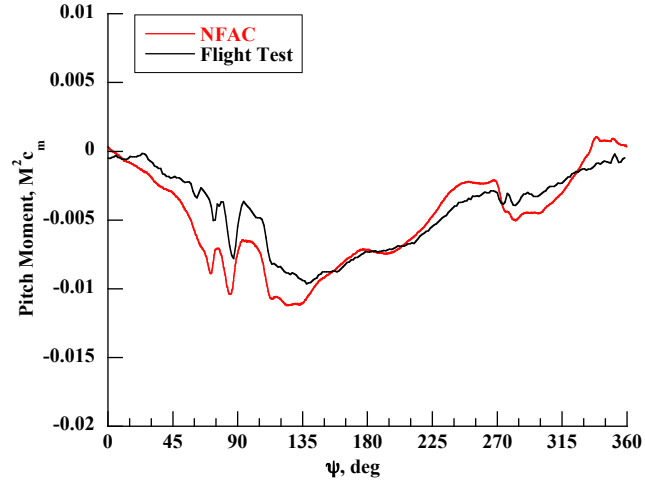

b) r/R=0.865

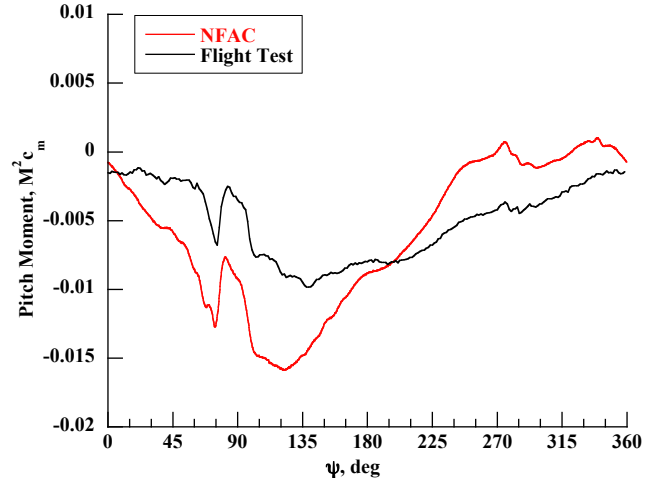

c) r/R=0.92

Figure 20. Comparison of NFAC section pitch moment (M^2c_m) with flight test (c8525, R60P18), r/R=0.225, 0.865, 0.920.

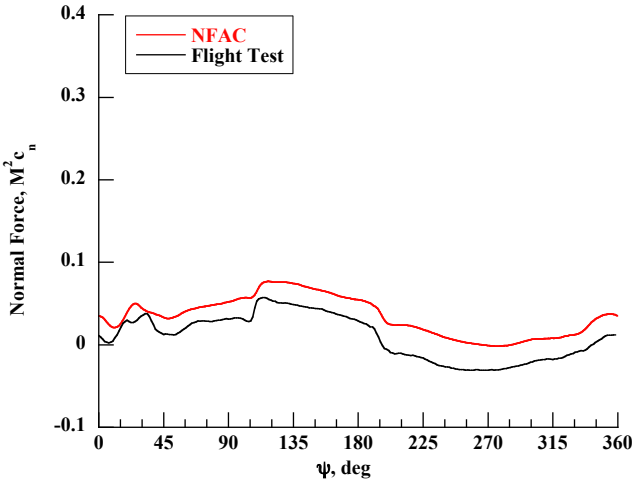

a) r/R=0.225

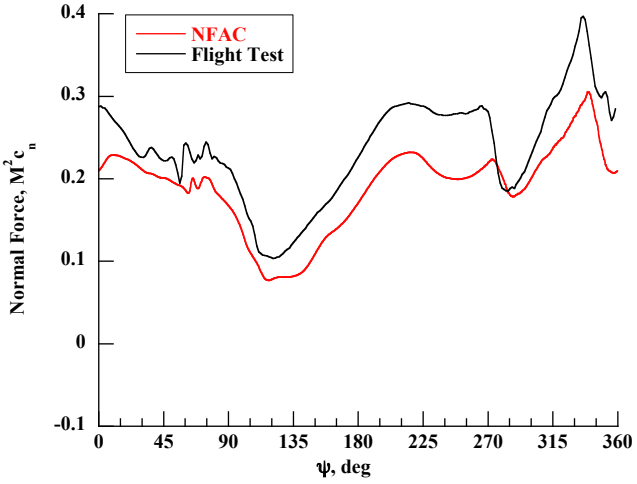

b) r/R=0.865

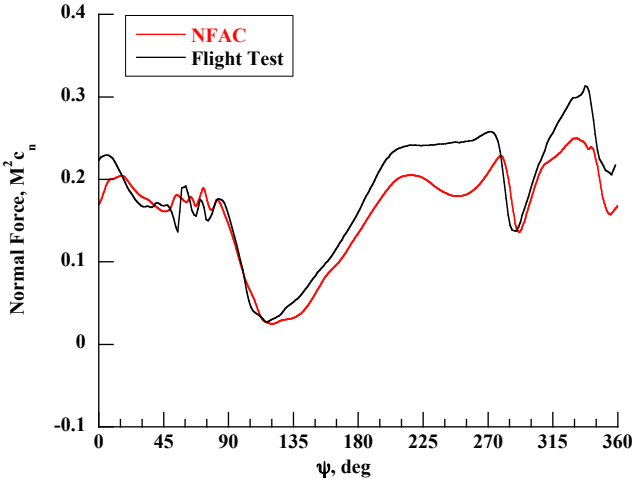

c) r/R=0.92

Figure 21. Comparison of NFAC section normal force (M^2c_n) with flight test (c9020, R60P28), r/R=0.225, 0.865, 0.920.

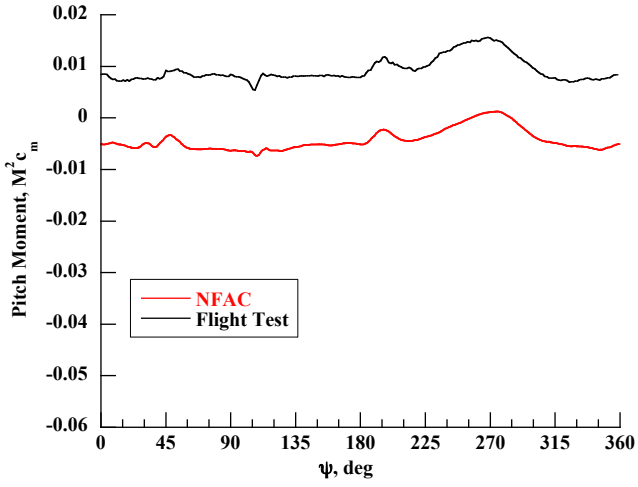

a) r/R=0.225

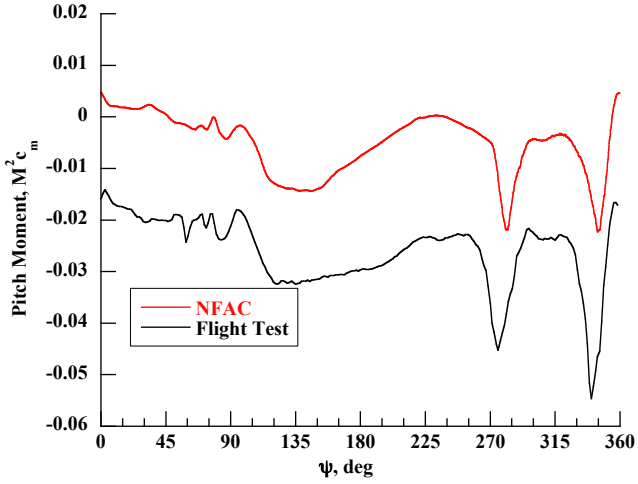

b) r/R=0.865

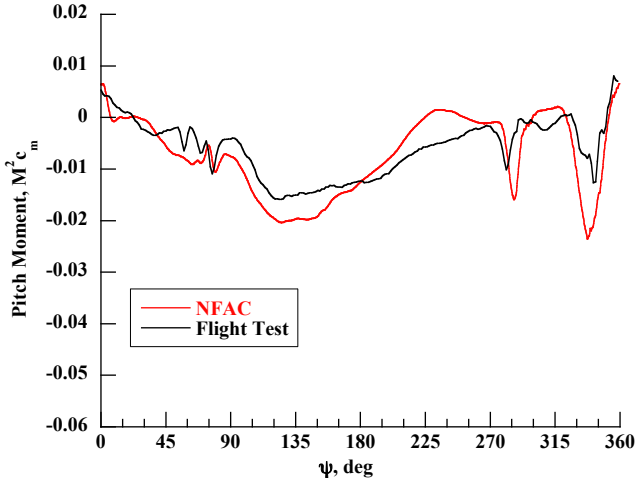

c) r/R=0.92

Figure 22. Comparison of NFAC section pitch moment (M^2c_m) with flight test (c9020, R60P28), r/R=0.225, 0.865, 0.920.

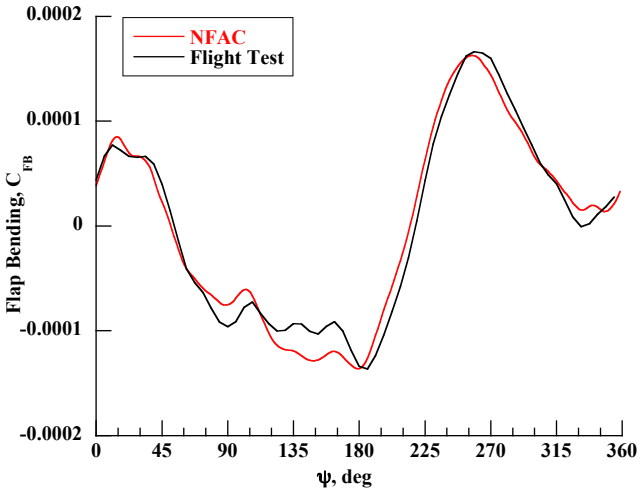

a) Flap Bending

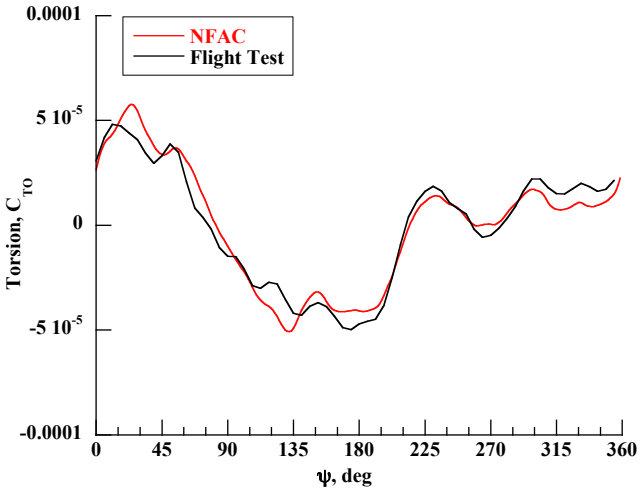

b) Torsion

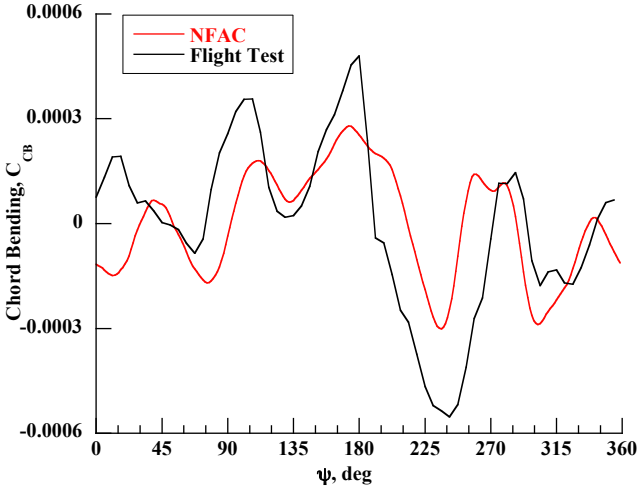

c) Chord Bending

Figure 23. Comparison of NFAC blade flap bending (r/R=0.60), torsion (r/R=0.30), and chord bending (r/R=0.60) with flight test (c8424, R47P21), means removed.

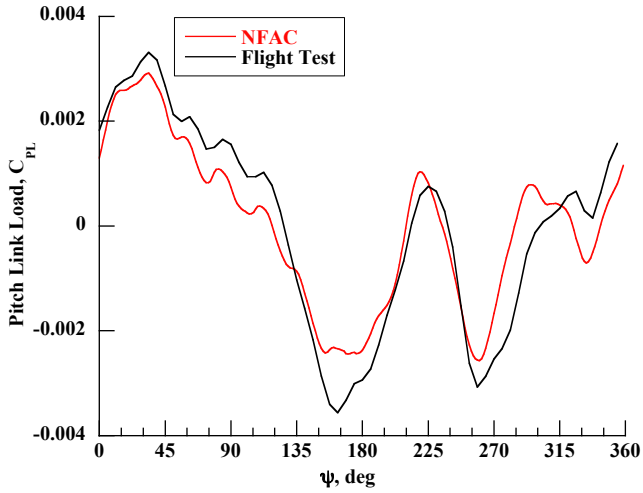

a) Pitch Link Load

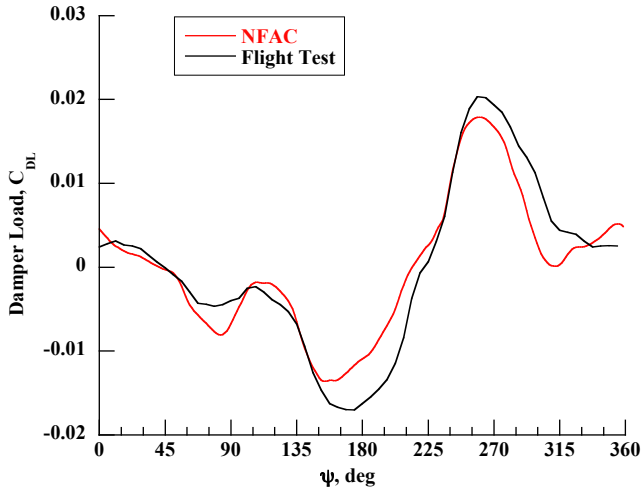

b) Damper Force

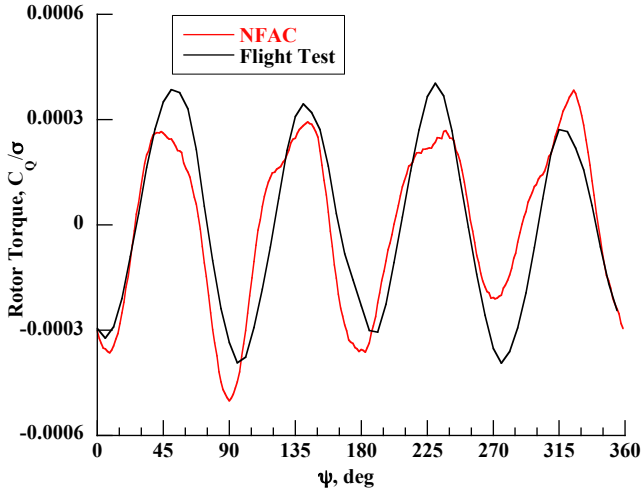

c) Torque

Figure 24. Comparison of NFAC pitch link load, damper force, and rotor torque with flight test (c8424, R47P21), means removed.

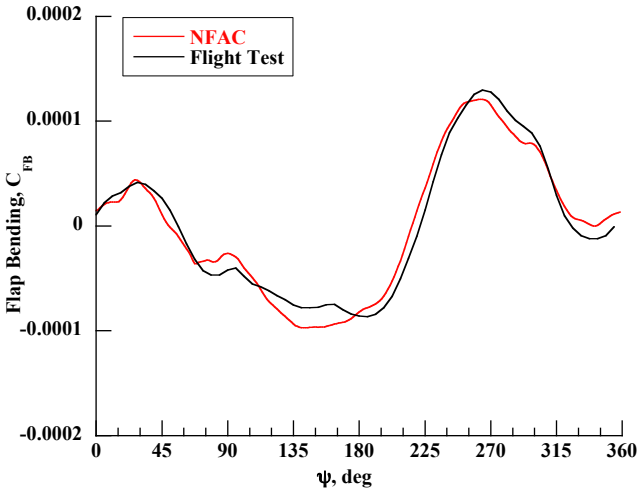

a) Flap Bending

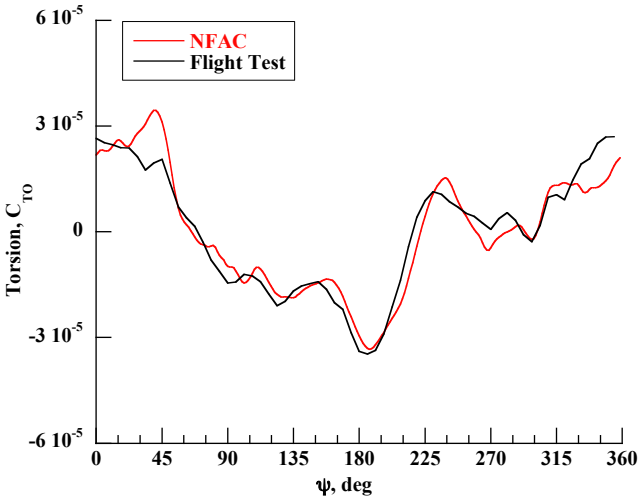

b) Torsion

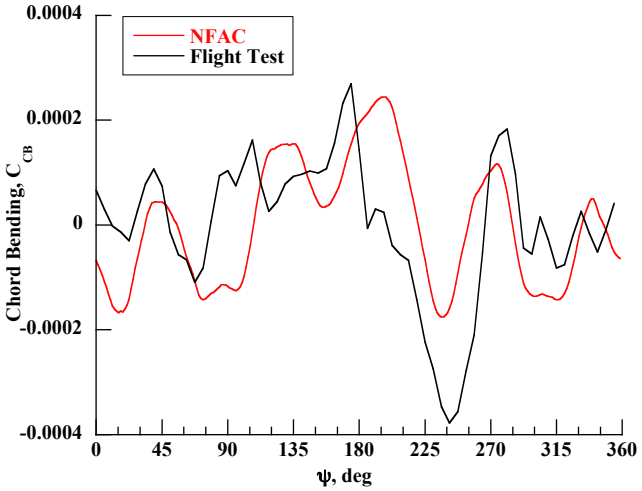

c) Chord Bending

Figure 25. Comparison of NFAC blade flap bending (r/R=0.60), torsion (r/R=0.30), and chord bending (r/R=0.60) with flight test (c8525, R60P18), means removed.

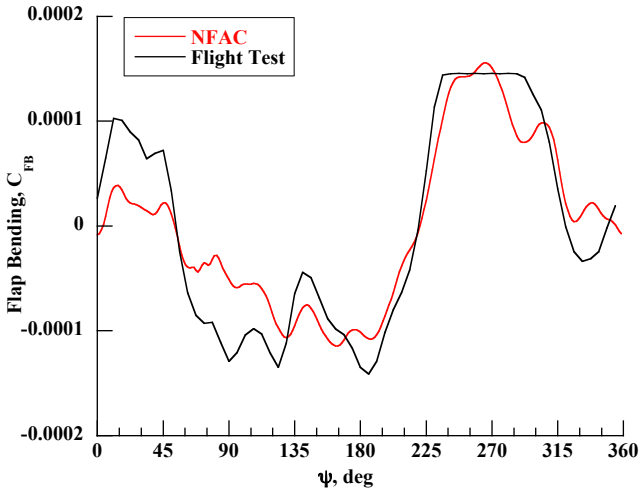

a) Flap Bending

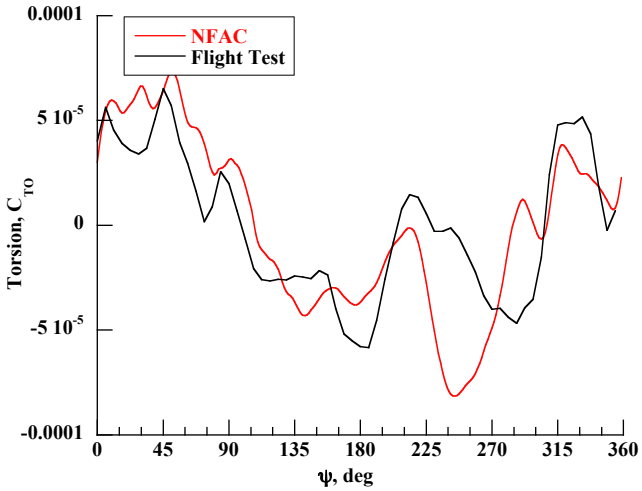

b) Torsion

Figure 26. Comparison of NFAC blade flap bending (r/R=0.60) and torsion (r/R=0.30) with flight test (c9020, R60P28), means removed.

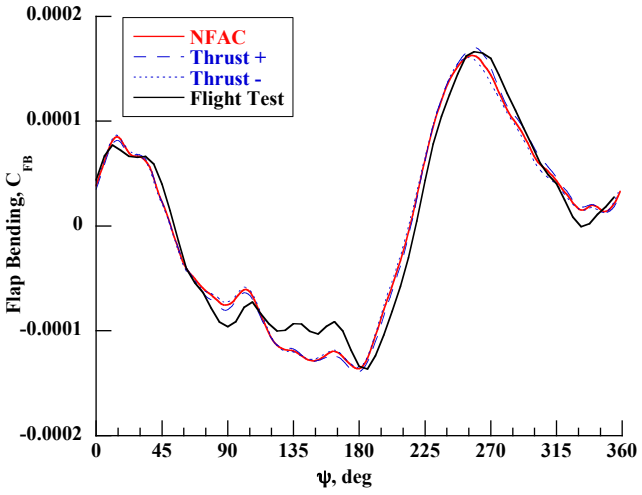

a) Thrust

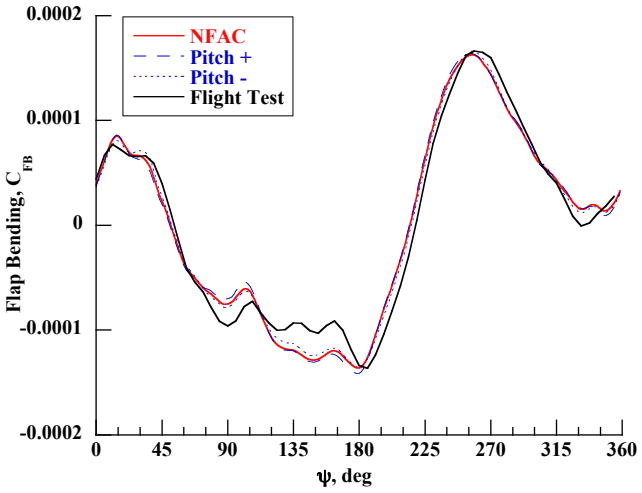

b) Hub Pitching Moment

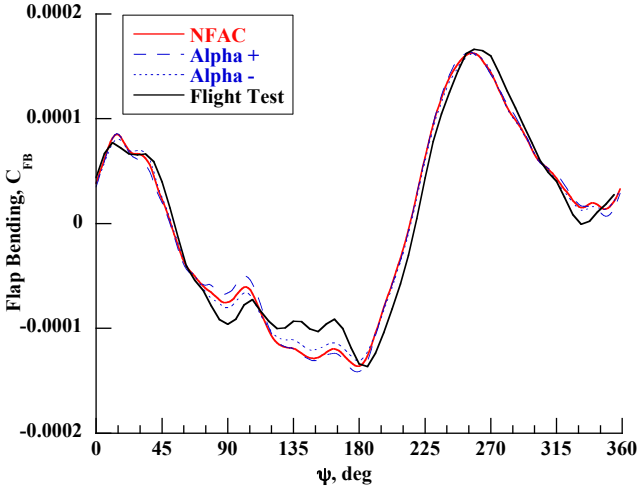

c) Shaft Angle

Figure 27. Effect of NFAC trim target derivatives on blade flap bending, c8424 simulation, r/R=0.60.

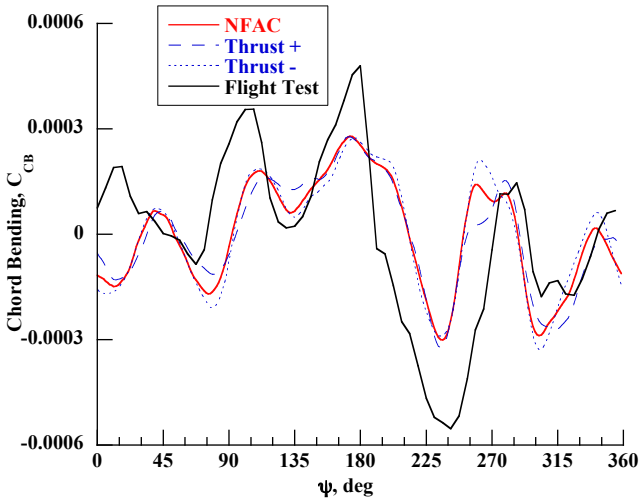

a) Thrust

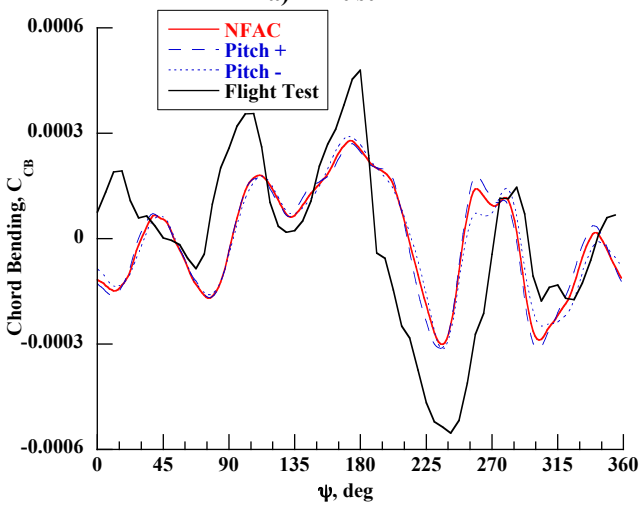

b) Hub Pitching Moment

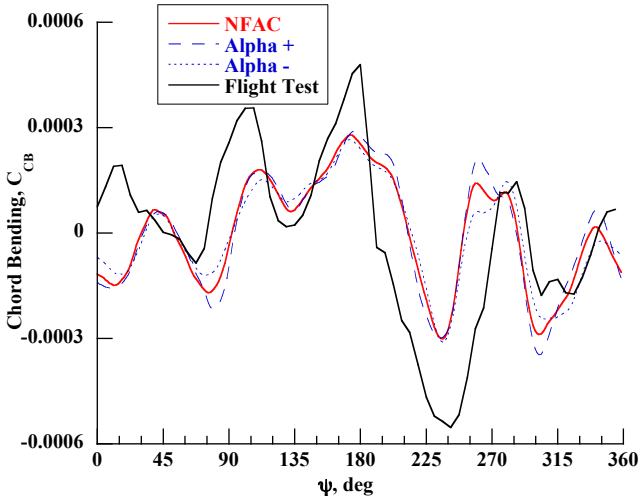

c) Shaft Angle

Figure 28. Effect of NFAC trim target derivatives on blade chord bending, c8424 simulation, r/R=0.60.

unlikely to be the cause of differences between NFAC and flight structural loads.

More complete comparisons of the flap bending, torsion and chord bending measurements are shown in Figs. 29-34. Figures 29 and 30 provide the magnitude and phase for the first 6 harmonics for all working flap bending gages as a function of radius. It is somewhat surprising (considering the good correlations shown in Fig. 27) that the flap bending magnitudes for the first 3 harmonics (Fig. 29) are not closer. In particular, the NFAC data has higher 1/rev and 2/rev magnitudes than flight, especially over the middle portion of the blade, while the flight test data has higher 3/rev magnitudes. The trends of magnitude as a function of radius are matched reasonably well, however. The phase results match quite well for these first 3 harmonics (Fig. 30), with slightly higher differences at 3/rev. The magnitudes for 4/rev-6/rev match well and are relatively small for all radial stations.

Figures 31 and 32 provide the magnitude and phase for the first 6 harmonics for all working blade torsion gages as a function of radius (note that only 3 torsion gages were working during the flight test). Based on these limited radial comparisons, the NFAC torsion magnitudes are somewhat higher than flight at 2/rev and 5/rev and match well for the other harmonics. The phase results match well for most harmonics, with some differences noted at 3/rev.

Figures 33 and 34 provide the magnitude and phase for the first 6 harmonics for all working chord bending gages as a function of radius. The differences between the NFAC and flight are clearly demonstrated in these figures. The flight test had higher 1/rev and 2/rev magnitudes for all radial stations. The 3/rev and 6/rev magnitudes matched well but the 4/rev and 5/rev were significantly different. In particular, the flight test had higher 4/rev magnitudes over the entire blade, while the wind tunnel had higher 5/rev magnitudes outboard of r/R=0.20. The trends of magnitude as a function of radius are matched reasonably well, however. In general, the phase trends matched well (Fig. 34) with the exception of 3/rev and 5/rev.

The differences in chord bending 1/rev and 2/rev are most likely due to differences in installed damper characteristics/response. The damper time history comparison (Fig. 24b) is consistent with this theory, and harmonic analysis (not shown) confirms these damper load differences are due to higher 1/rev and 2/rev magnitudes for the flight test. The significant differences at 4/rev and 5/rev are not currently understood. However, since the first elastic lag frequency is predicted to be 4.7/rev (Fig. 4), it is possible that any change in the chord frequencies between flight and NFAC could change the 4/rev and 5/rev magnitudes considerably. Differences between flight and NFAC that could affect these frequencies include the drive train dynamics and in-plane hub motion. It is recommended that the potential effects of these differences be further investigated.

DNW Test Simulation

Power

Figure 35 shows a comparison of non-dimensional rotor power (C_P/σ) for the three DNW test conditions (13.20, 11.24, 13.12). Similar to Fig. 8, the DNW rotor power is compared to the one representative NFAC baseline point, the average from all NFAC baseline points, and to the average corrected power.

The effects of trim changes on rotor power are shown for one simulated DNW condition (13.20) in Fig. 36. These data show that longitudinal flapping, thrust, and shaft angle all have significant effects on power, as expected.

For the 13.20 comparisons in Fig. 35, the NFAC baseline and averaged baseline power is 3% higher ($\Delta C_P/\sigma$=+0.0002) than the DNW. After correction (predominantly for the effects of thrust), the NFAC power is virtually identical. For the 11.24 and 13.12 simulations, the NFAC baseline power was 8% and 2% lower respectively ($\Delta C_P/\sigma$=-0.0001 and -0.00005). Because the baseline conditions were so close to targets for these simulations, corrections had minimal effect.

The good agreement between small- and full-scale rotor power is somewhat surprising. It is generally expected (Ref. 14) that a scale model would have higher drag (and higher power required) than a full-scale rotor due to its reduced Reynolds number. The current results, as well as previous full-scale comparisons with the DNW data (Ref. 15), do not show this effect. Thus it is possible that the small-scale DNW model blades were unusually smooth and compensated for the effects of Reynolds number. Nevertheless, the consistency of the power measurements suggests that the DNW matching method used during the NFAC test was fundamentally sound.

Airloads

The rotor airloads are investigated in this section, with the primary emphasis on the 13.20 condition. For these comparisons, data from the NFAC baseline condition (R47P40) were used.

Figure 37 shows the normal force distribution along the blade and around the azimuth for the 13.20 DNW test condition. Because of the similarity in flight conditions, this radial contour plot shows the same features as were seen in Fig. 8 for the flight test, including negative lift near the tip in the second quadrant and on the inboard sections of the retreating blade. Figure 38 shows the difference in normal force distribution between the DNW and NFAC tests for this condition. The DNW rotor provides less lift behind the rotor and in the negative lift portion of the second quadrant and more lift in the first and third quadrants. The 3/rev character of the lift difference is readily apparent in this figure. More detailed lift distributions are provided in Figs. 39-42.

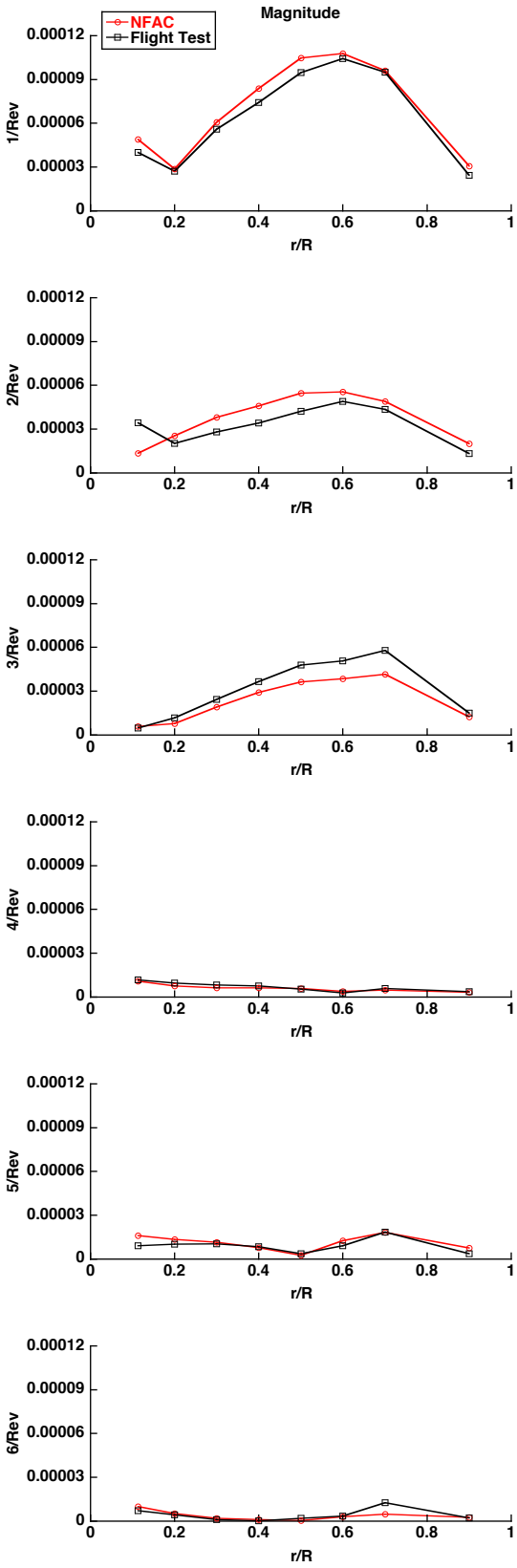

Figure 29. Comparison of NFAC blade flap bending (C_{FB}) harmonic magnitudes with flight test (c8424, R47P21).

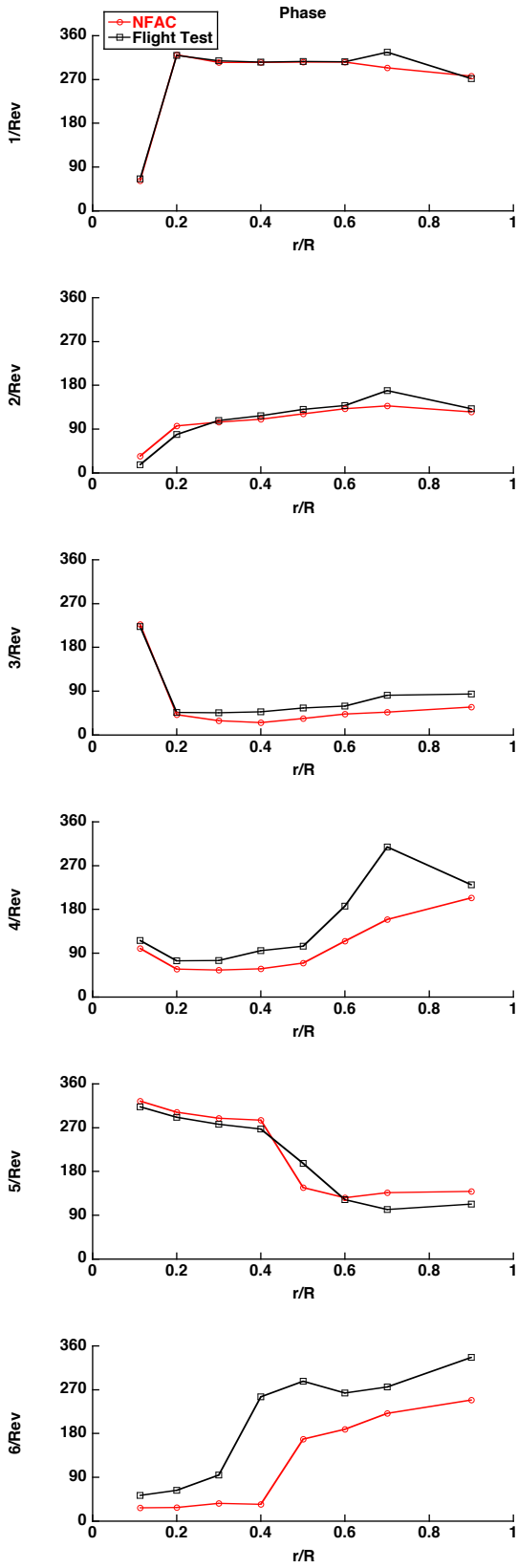

Figure 30. Comparison of NFAC blade flap bending (C_{FB}) harmonic phases with flight test (c8424, R47P21).

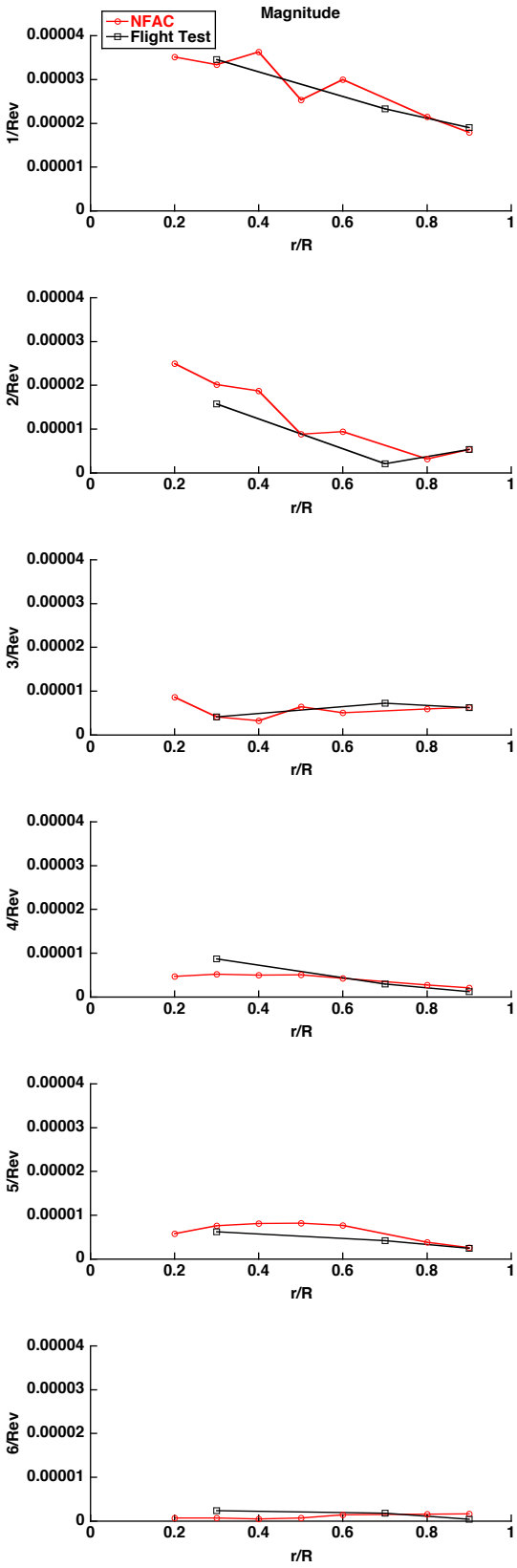

Figure 31. Comparison of NFAC blade torsion (C_{TO}) harmonic magnitudes with flight test (c8424, R47P21).

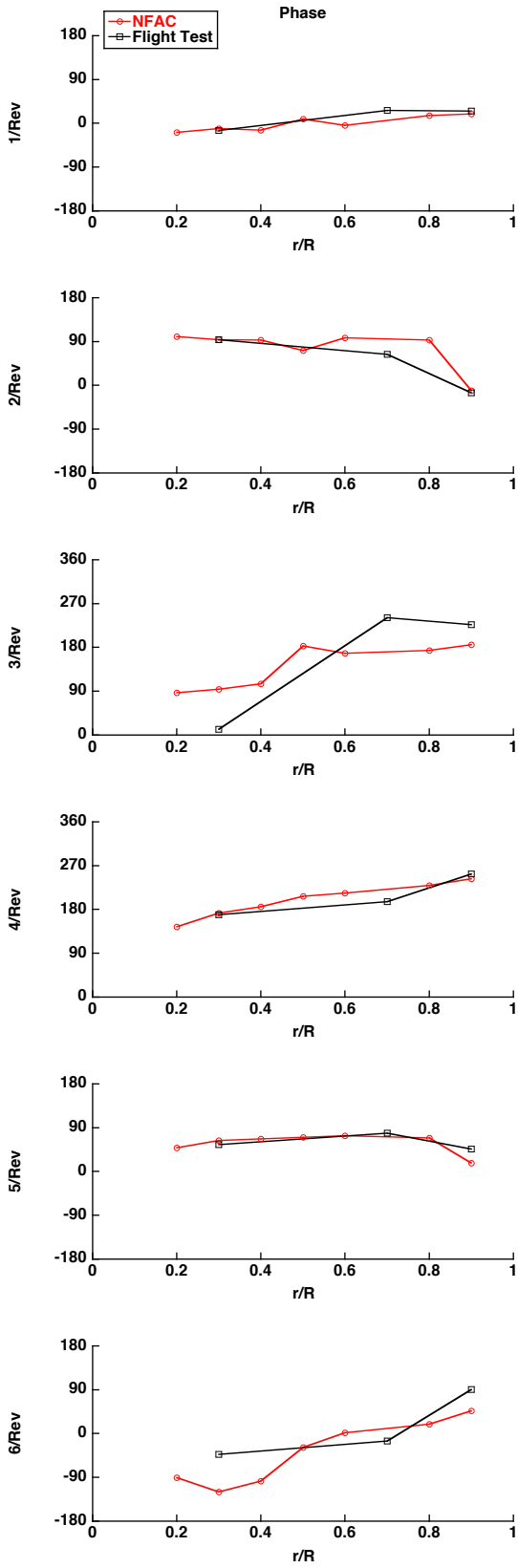

Figure 32. Comparison of NFAC blade torsion (C_{TO}) harmonic phases with flight test (c8424, R47P21).

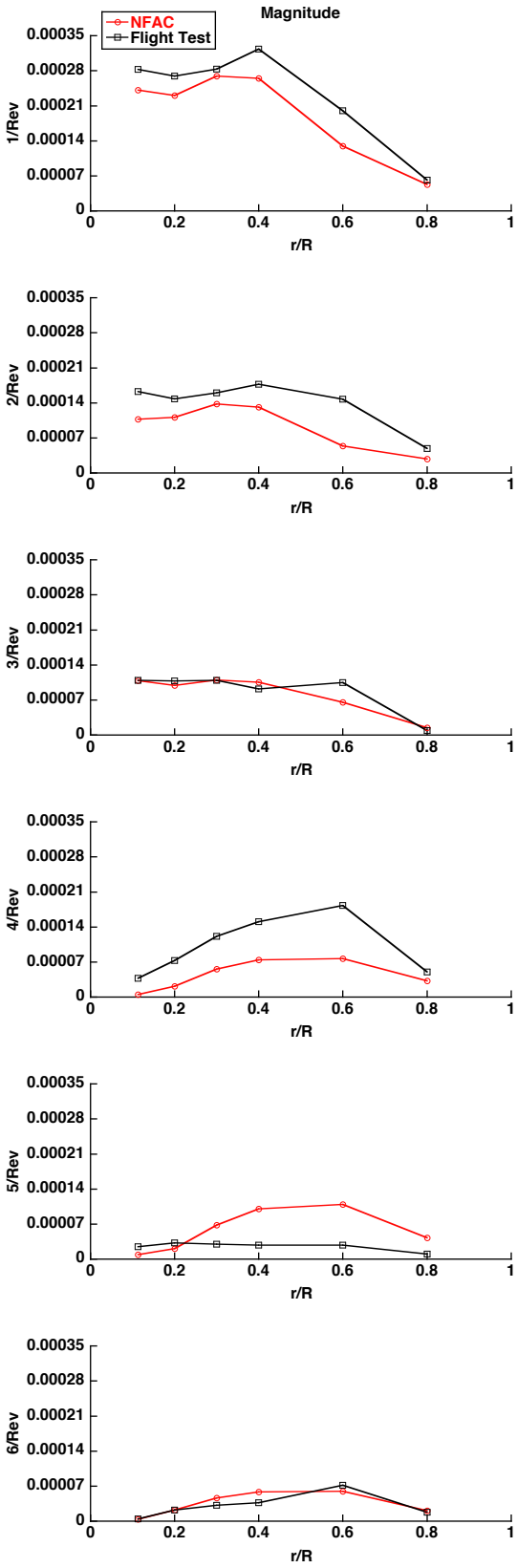

Figure 33. Comparison of NFAC blade chord bending (C_{CB}) harmonic magnitudes with flight test (c8424, R47P21).

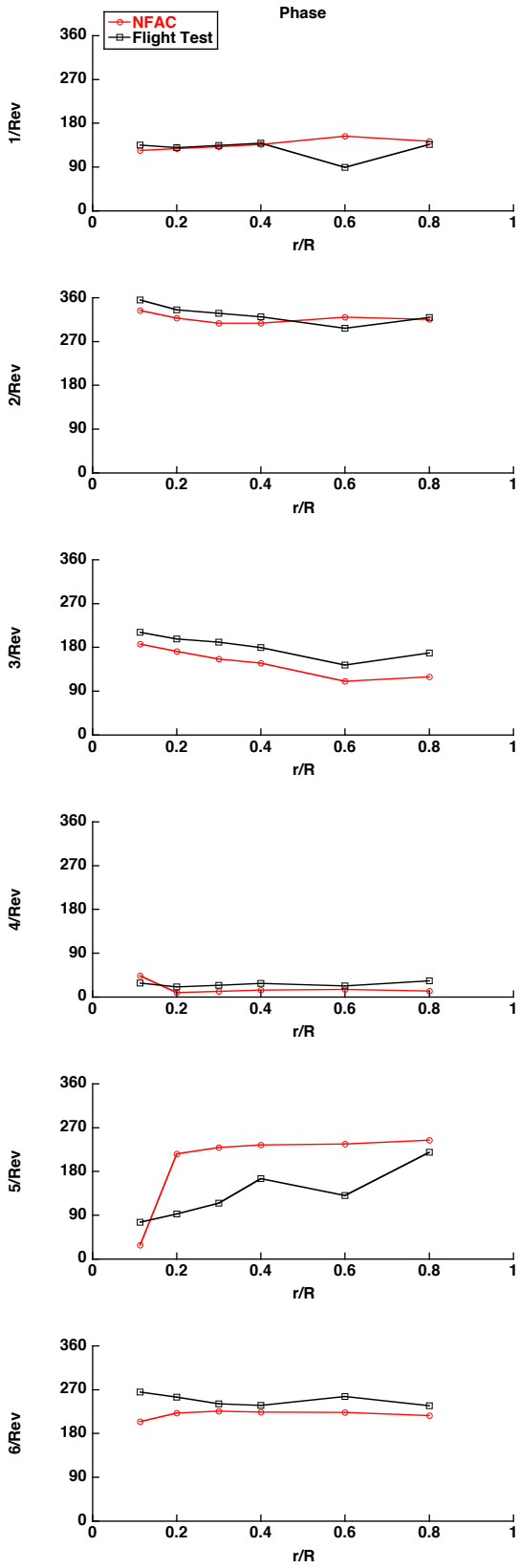

Figure 34. Comparison of NFAC blade chord bending (C_{CB}) harmonic phases with flight test (c8424, R47P21).

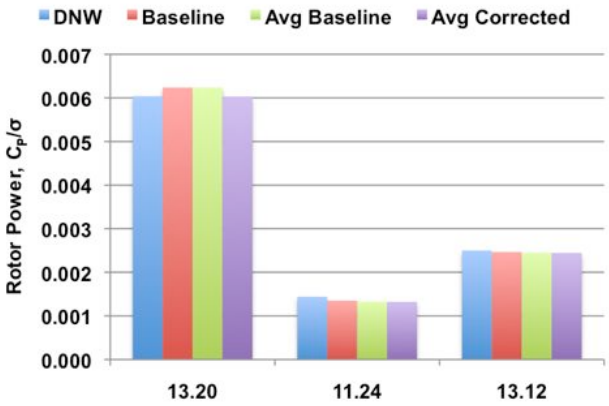

Figure 35. Comparison of NFAC rotor power with DNW test for three forward flight conditions.

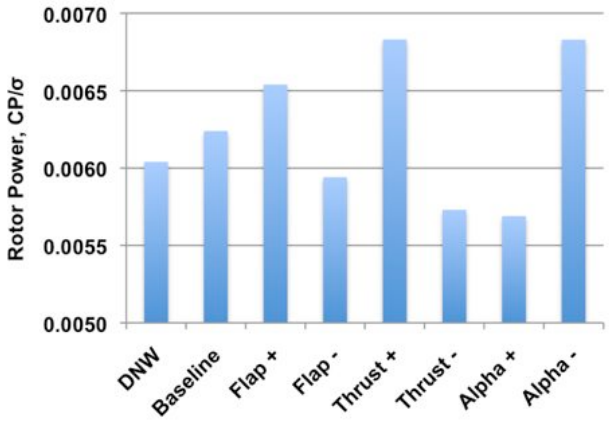

Figure 36. Effect of NFAC trim target derivatives on rotor power for one DNW condition (13.20 simulation).

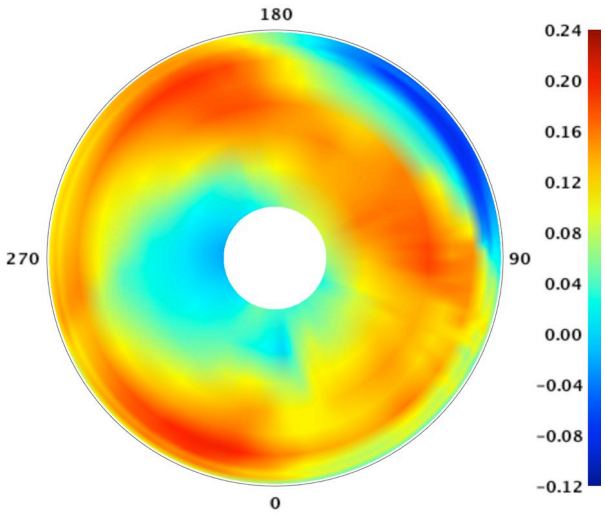

Figure 37. Section normal force distribution (M^2c_n) for DNW test condition (13.20).

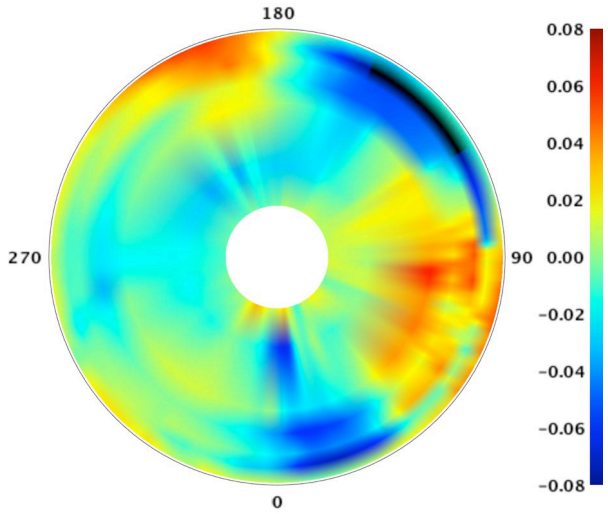

Figure 38. Difference in section normal force distribution (M^2c_n) between DNW test (13.20) and NFAC (R47P40).

Figures 39 and 40 show the non-dimensional normal force and pitch moment for r/R=0.225, 0.40, and 0.775. There is good agreement for the normal force at the two inboard stations (Fig. 39), with slightly higher NFAC force levels on the retreating side for r/R=0.40. The moments at these stations are similar in shape, with slightly higher DNW magnitudes at r/R=0.225 and a steady offset at r/R=0.40. At r/R=0.775, we start to see significant differences in the normal force, with the DNW data showing less lift behind the rotor and in the second quadrant. Similar to the flight test comparison, the NFAC data also show a reduced rate of change of normal force between ψ=120 and 240 deg. The moments at r/R=0.775 show some differences, but the overall magnitudes are small.

These same normal force trends are seen at the remaining outboard stations (Fig. 41). Considering the differences in normal forces, the moments at the outboard stations (Fig. 42) compare favorably, with the exception of magnitude differences at r/R=0.92.

As was done for the flight test comparisons, the sensitivity of the airload results to trim conditions was evaluated. Trim variations included longitudinal flapping, thrust, and shaft angle. Similar to the results shown in Figs. 14 and 15, the trim variations had only a minimal effect on the airloads (not shown). This suggests that trim target errors are unlikely to be the cause of the differences between the DNW and NFAC airloads.

Previous comparisons between DNW and flight test data (Refs. 2, 9) suggested that the lower DNW lift behind the rotor was likely caused by the relatively larger instrumentation hat used during DNW testing. Many of the

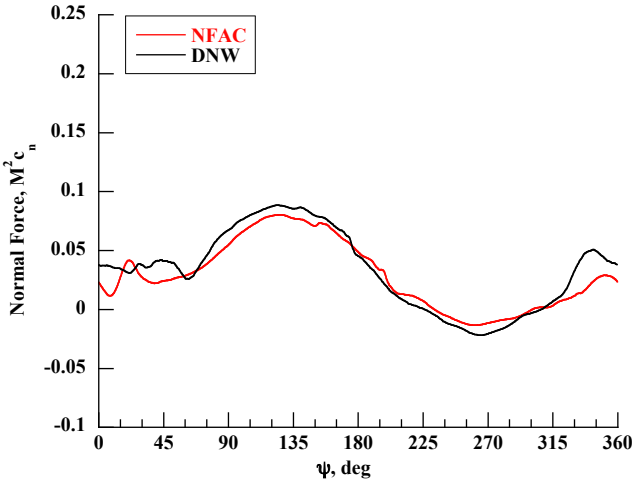

a) r/R=0.225

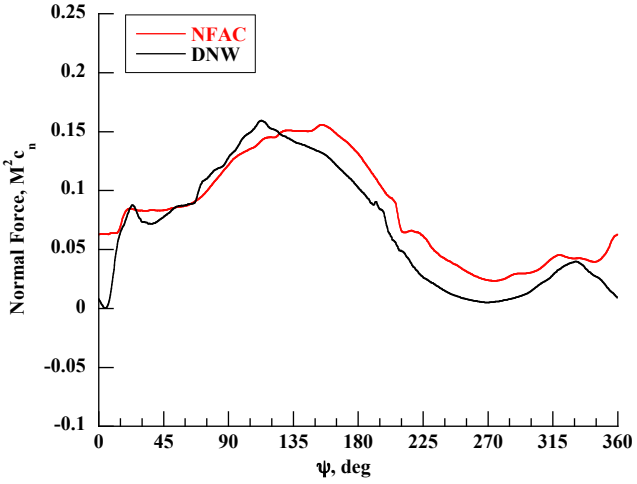

b) r/R=0.40

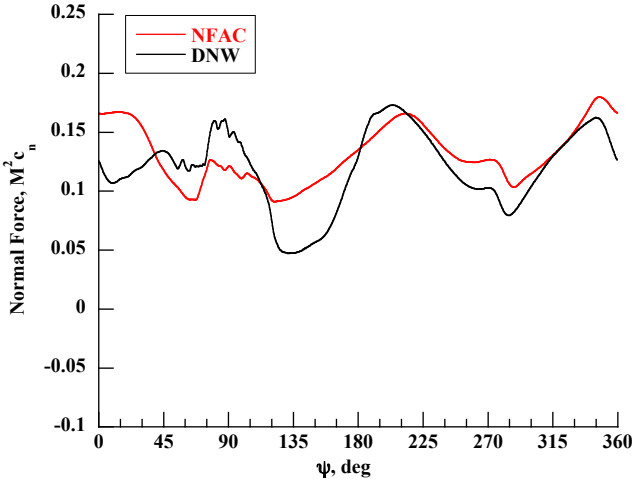

c) r/R=0.775

Figure 39. Comparison of NFAC section normal force (M^2c_n) with DNW test (13.20, R47P40), r/R=0.225, 0.400, 0.775.

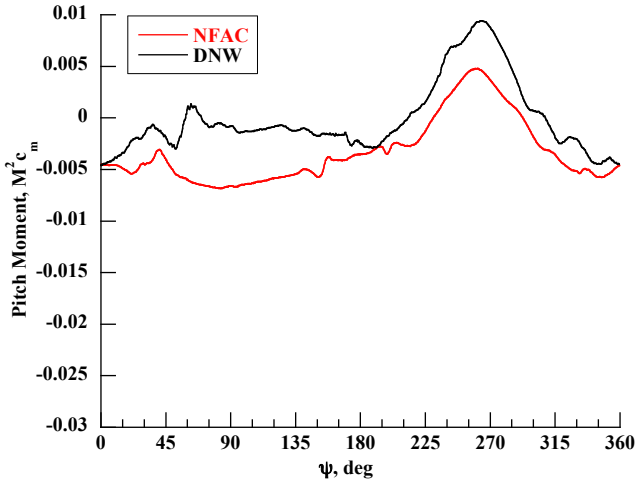

a) r/R=0.225

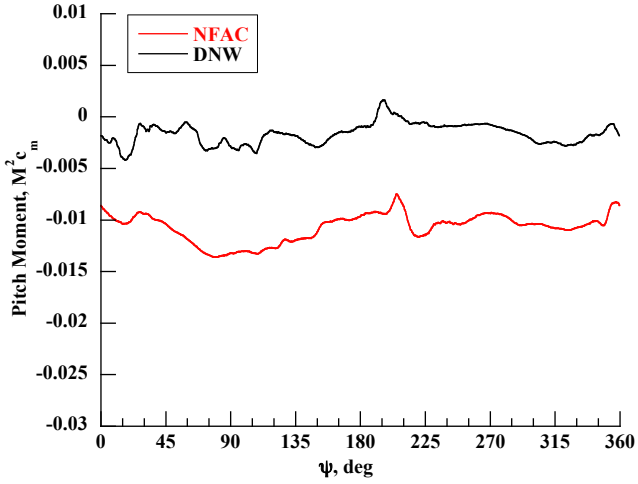

b) r/R=0.40

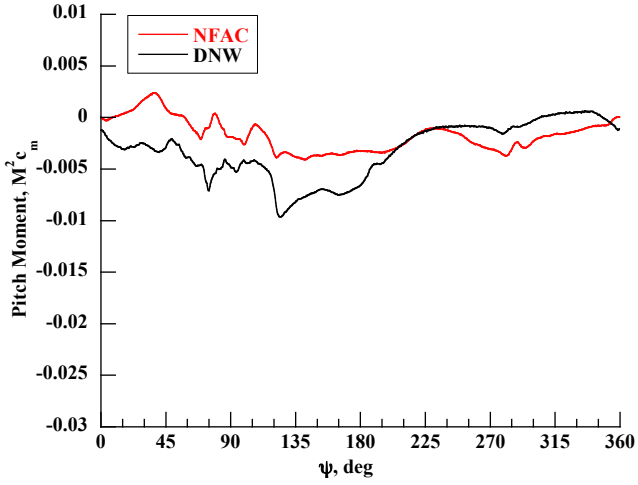

c) r/R=0.775

Figure 40. Comparison of NFAC section pitch moment (M^2c_m) with DNW test (13.20, R47P40), r/R=0.225, 0.400, 0.775.

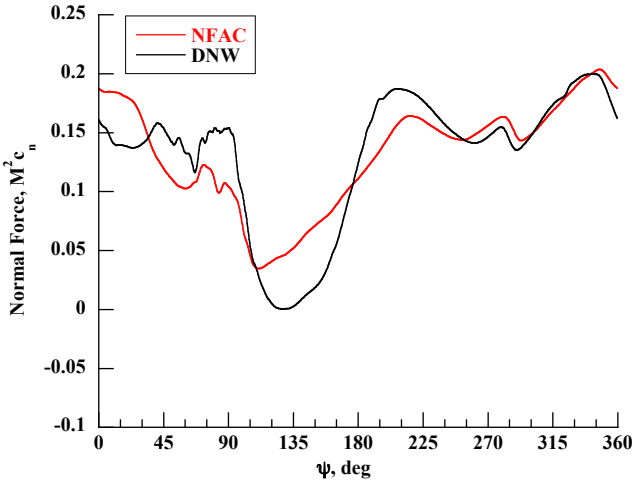

a) r/R=0.865

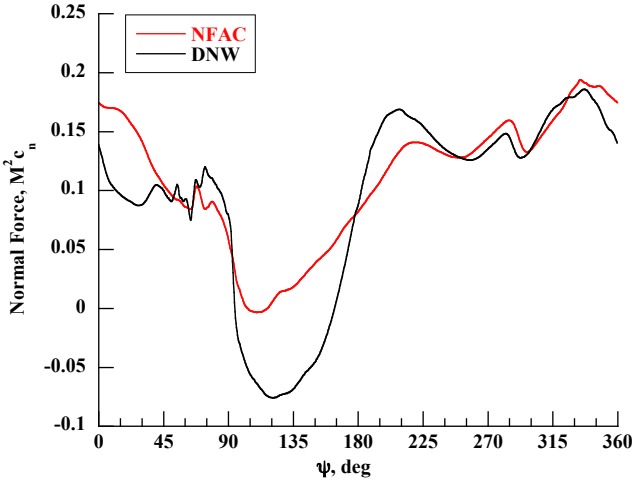

b) r/R=0.92

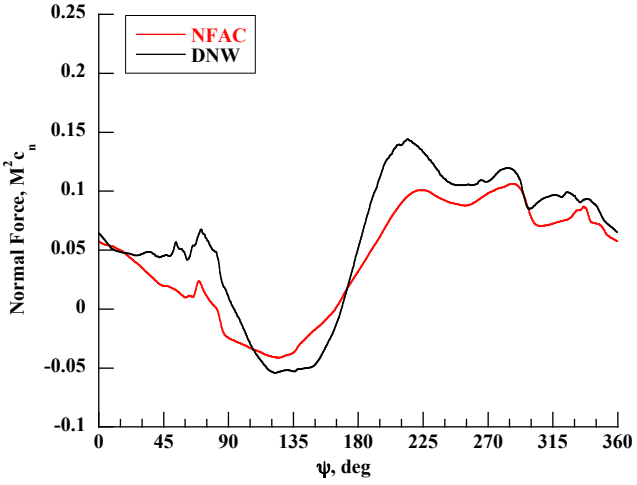

c) r/R=0.99

Figure 41. Comparison of NFAC section normal force (M^2c_n) with DNW test (13.20, R47P40), r/R=0.865, 0.920, 0.990.

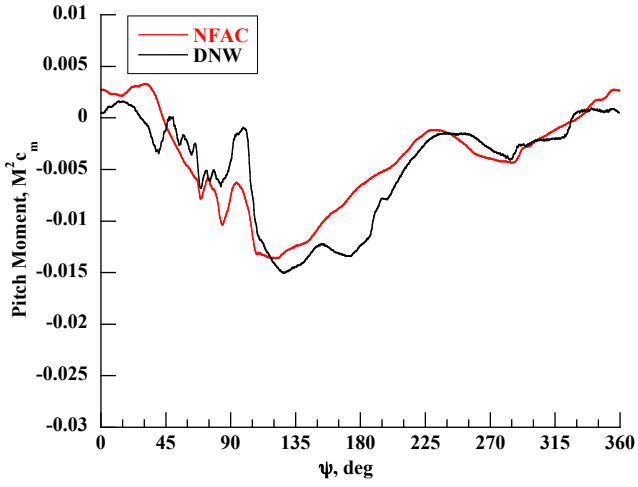

a) r/R=0.865

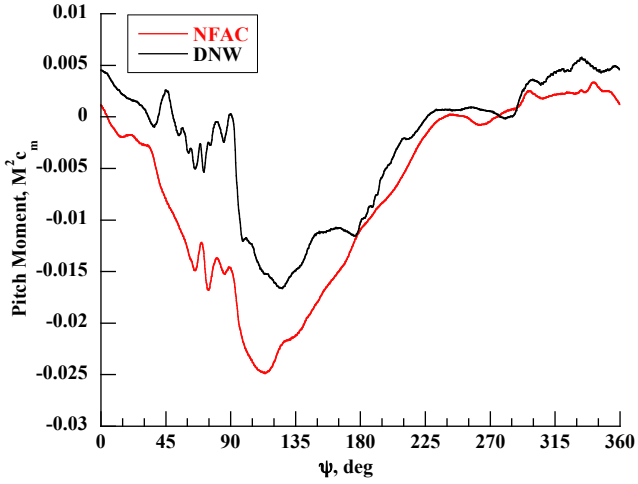

b) r/R=0.92

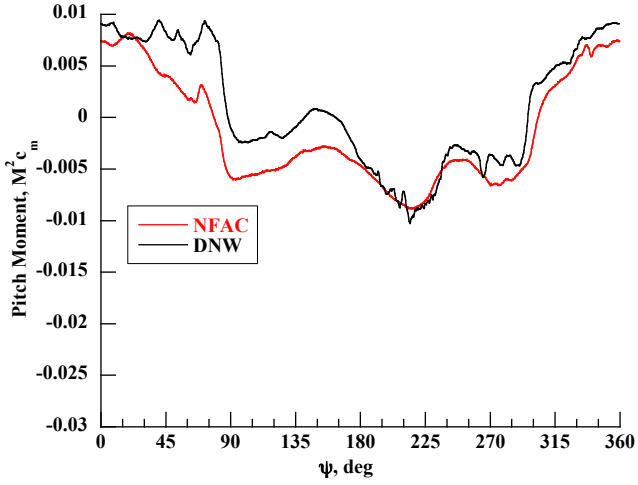

c) r/R=0.99

Figure 42. Comparison of NFAC section pitch moment (M^2c_m) with DNW test (13.20, R47P40), r/R=0.865, 0.920, 0.990.

other differences may be the result of differences in the blade torsional properties between the small- and full-scale blades (discussed earlier and in Ref. 10), with the DNW model having a torsional natural frequency much closer to 3/rev. This would result in greater aeroelastic coupling and an increased 3/rev loading.

Structural Loads

The rotor structural loads for the 13.20 condition are investigated in this section. For these comparisons, data from the NFAC baseline condition (R47P40) were used.

Sample comparisons of blade bending time histories (with means removed) for the 13.20 test condition are provided in Fig. 43. Blade flap bending, torsion, and chord bending are shown at nominally equivalent radial stations (r/R=0.35 for DNW, r/R=0.30 for NFAC). Even though the peak-to-peak magnitudes are similar for these measurements, there are considerable differences in the waveforms, especially for torsion and chord bending.

More complete comparisons of the flap and chord bending measurements are provided in Figs. 44-49. Figures 44 and 45 provide the magnitude and phase for the first 6 harmonics for the flap bending gages as a function of radius. The NFAC data has higher 1/rev and 2/rev magnitudes than the DNW, especially over the middle portion of the blade, while the DNW data has higher 3/rev and 4/rev magnitudes. The phase results match well at 1/rev with larger differences at the higher harmonics. The magnitudes for 5/rev and 6/rev match well and are relatively small for all radial stations.

Figures 46 and 47 provide the magnitude and phase for the first 6 harmonics for the blade torsion gages as a function of radius. The DNW shows higher magnitudes for all harmonics except 2/rev, with the biggest differences seen at 3/rev and 4/rev. There are small phase differences for most harmonics, with the largest at 3/rev.

Figures 48 and 49 provide the magnitude and phase for the first 6 harmonics for the chord bending gages as a function of radius. The NFAC data has higher 1/rev and 2/rev magnitudes than the DNW, especially over the inboard part of the blade. The 3/rev and 6/rev match well, and the 5/rev varies with radial station. The DNW has significantly higher 4/rev magnitudes over the entire blade. In general, the phase trends match well although there are noticeable offsets at the higher harmonics.

The significant differences in blade bending measurements (especially 3/rev torsion) between the DNW and the NFAC provide additional verification that the different blade modal properties of the DNW model had a significant effect on blade response and ultimately, blade airloads. The results are similar to earlier DNW/flight test comparisons even with the elimination of uncertainties with rotor trim conditions (and trim method).

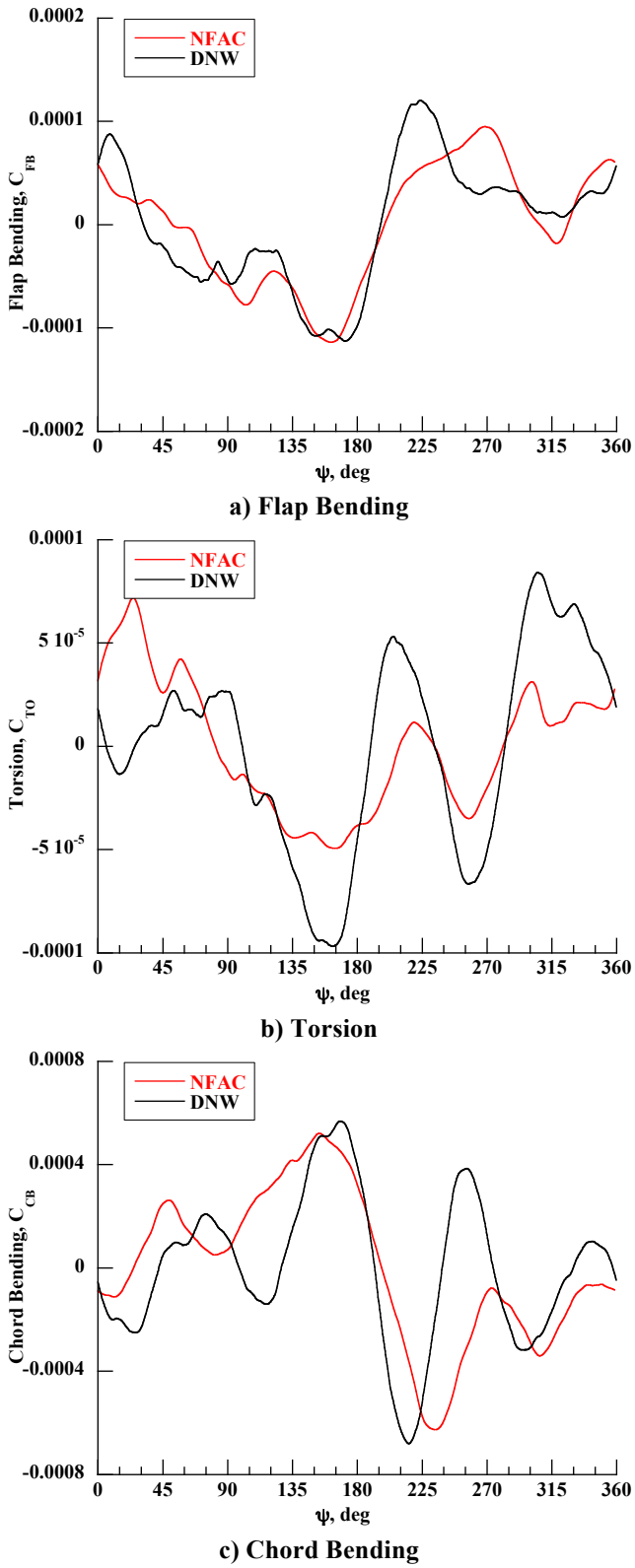

Figure 43. Comparison of NFAC blade flap bending, torsion, and chord bending with DNW test, r/R=0.30 (NFAC), r/R=0.35 (DNW), (13.20, R47P40), means removed.

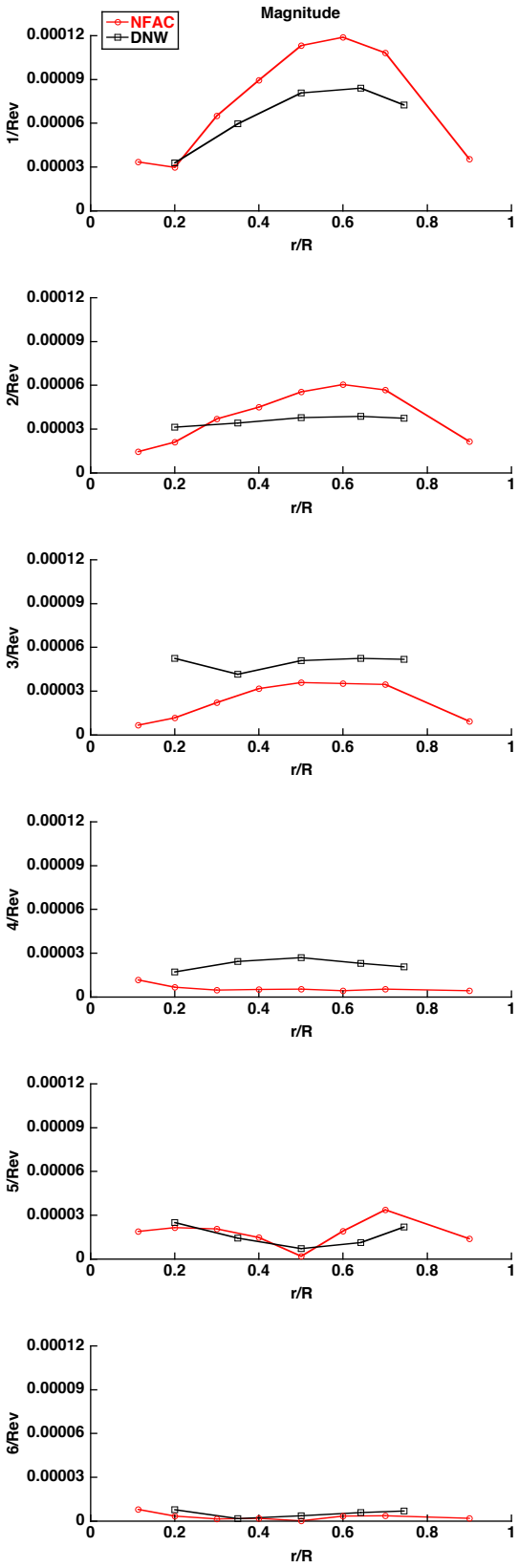

Figure 44. Comparison of NFAC blade flap bending (C_{FB}) harmonic magnitudes with DNW test (13.20, R47P40).

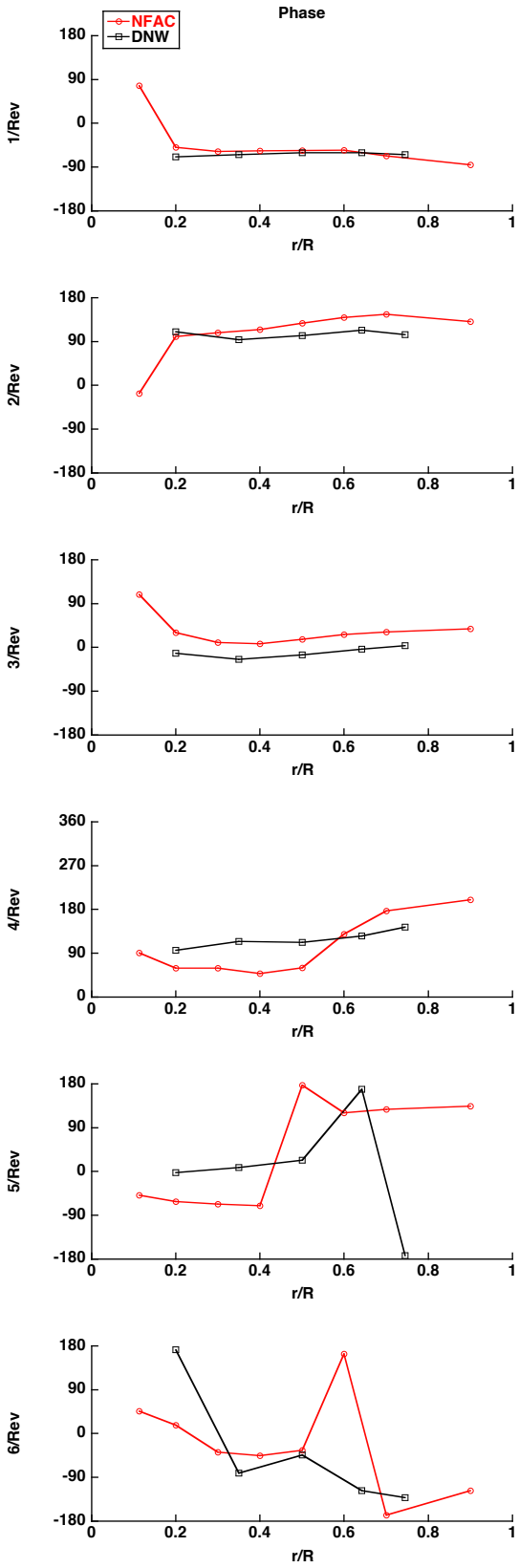

Figure 45. Comparison of NFAC blade flap bending (C_{FB}) harmonic phases with flight test (13.20, R47P40).

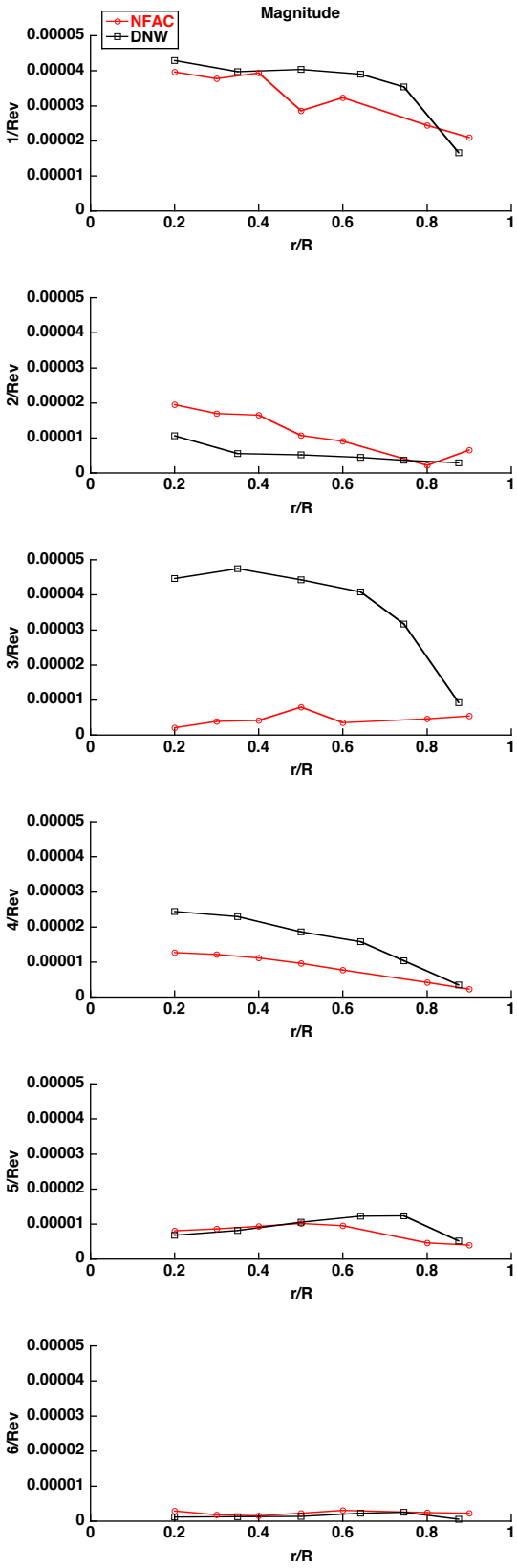

Figure 46. Comparison of NFAC blade torsion (C_{TO}) harmonic magnitudes with DNW test (13.20, R47P40).

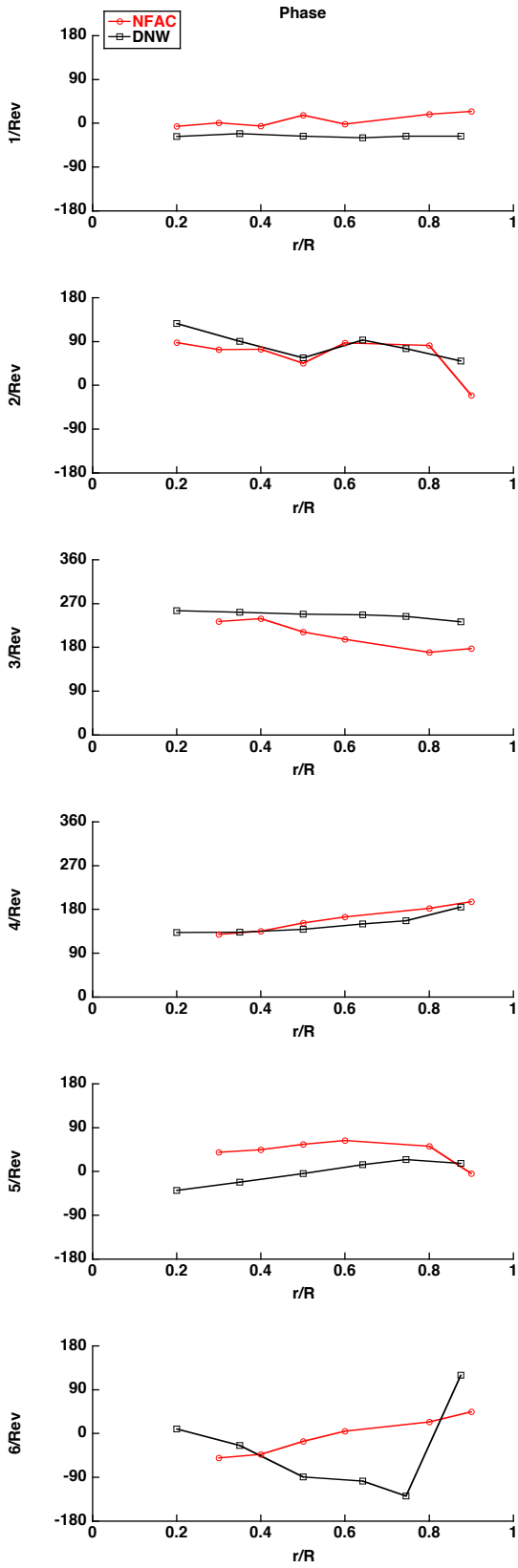

Figure 47. Comparison of NFAC blade torsion (C_{TO}) harmonic phases with DNW test (13.20, R47P40).

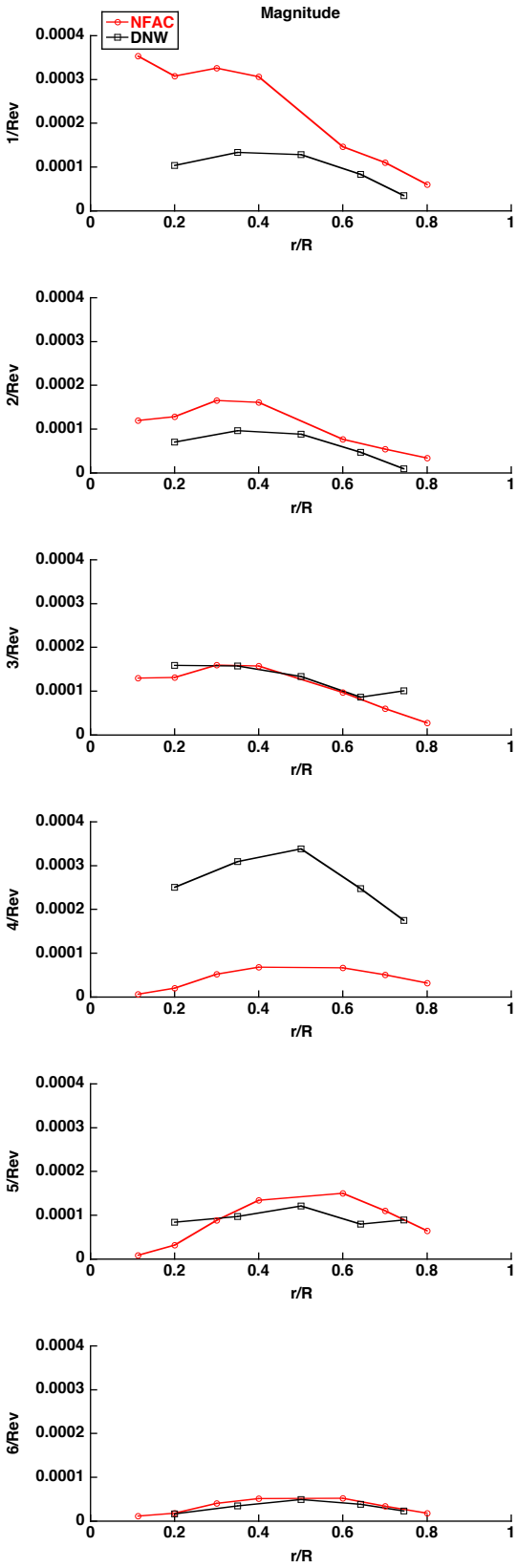

Figure 48. Comparison of NFAC blade chord bending (C_{CB}) harmonic magnitudes with DNW test (13.20, R47P40).

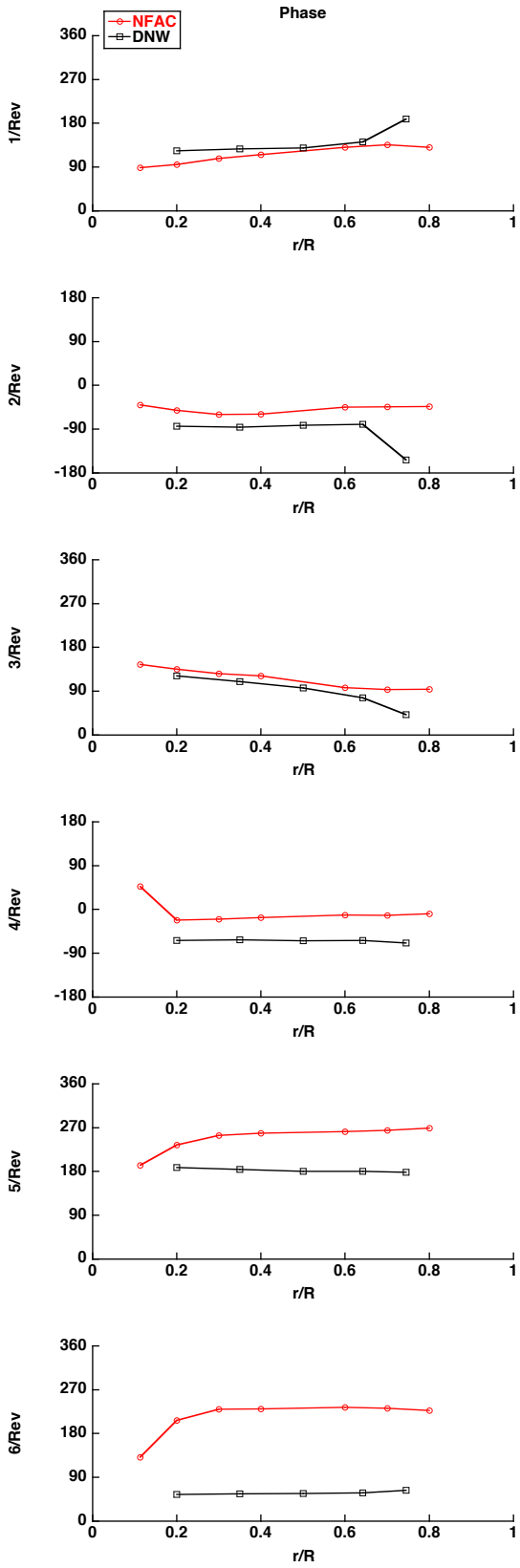

Figure 49. Comparison of NFAC blade chord bending (C_{CB}) harmonic phases with DNW test (13.20, R47P40).

CONCLUSIONS

Three flight conditions and three DNW data points were simulated during the UH-60A Airloads Wind Tunnel test to investigate the effects of wind tunnel and model scale on rotor power, airloads, and structural loads. Conclusions from these flight test and DNW comparisons are provided below.

Flight Test

1) The procedures used to match flight test conditions were fundamentally sound. These included matching non-dimensional parameters for thrust, hub moments, and corrected shaft angle. This latter term included a mean flow angle change based on a simple Glauert-type correction.
2) The rotor power measurements compared favorably with flight test for all three test conditions (maximum error of 3.5%), yet the differences aren't consistent with a single error source in setting the rotor trim conditions (higher flight test thrust, more wind tunnel angle corrections, etc).
3) Rotor airloads (normal force and moment) are generally well simulated in the wind tunnel and trim variations have little effect. There are some noticeable differences in the waveforms, however, that can't be explained by bad measurements or integration errors. The physical cause of these differences is not currently known. The proximity of the wind tunnel walls to the rotor during testing is the most likely cause, but differences in turbulence levels or aero/structure coupling could also be contributing factors. It is recommended that these differences be investigated computationally, comparing results both with and without the wind tunnel modeled.
4) Rotor structural load time histories are also generally well simulated with the exception of blade chord bending. Trim variations have little effect on the structural load waveforms. The primary differences in chord bending were higher 4/rev and lower 5/rev magnitudes for the flight test. The reasons for these differences are not currently known but could be caused by blade chord frequency changes due to installation and hardware differences. It is recommended that the potential of these differences to affect the chord frequencies be investigated.

DNW Test

1) The procedures used to match the DNW conditions were fundamentally sound. These included matching non-dimensional parameters for thrust, 1/rev flapping, and corrected shaft angle. This latter term included a mean flow angle correction for both wind tunnels.
2) The rotor power measurements compared favorably with flight test for all three test conditions (errors of 0-8%). The good agreement between small- and full-scale power is somewhat surprising since the lower Reynolds number on the DNW blades were expected to have a larger effect.
3) Rotor airloads (normal force and moment) show significant differences in waveform, especially at the outboard radial stations. These differences are consistent with those found during earlier DNW/flight test comparisons.
4) The significant differences in blade bending measurements (especially torsion) between the DNW and the NFAC provide additional verification that the different blade modal properties of the DNW model had a significant effect on blade response and ultimately, blade airloads. The results are similar to earlier DNW/flight test comparisons even with the elimination of uncertainties with rotor trim conditions (and trim method).

REFERENCES

1. Norman, T. R., Shinoda, P., Peterson, R. L., and Datta, A., "Full-Scale Wind tunnel Test of the UH-60A Airloads Rotor," American Helicopter Society 67th Annual Forum, Virginia Beach, VA, May 2011.

2. Kufeld, R. M., Balough, D. L., Cross, J. L., Studebaker, K. F., Jennison, C. D., and Bousman, W. G., "Flight Testing of the UH-60A Airloads Aircraft," American Helicopter Society 50th Annual Forum, Washington D.C., May 1994.

3. Bousman, W. G., and Kufeld, R. M., "UH-60A Airloads Catalog," NASA TM-2005-212827, 2005.

4. Yu, Y. H., Liu, S. R., Landgrebe, A. J., Lorber, P. F., Pollack, M. J., Martin, R. M., and Jordan, D., "Aerodynamic and Acoustic Test of a United Technologies Model Scale Rotor at DNW," American Helicopter Society 46th Annual Forum, Washington, D.C., May 1990.

5. Lorber, P. F., "Aerodynamic Results of a Pressure-Instrumented Model Rotor Test at the DNW," Journal of the American Helicopter Society, Vol. 36, (4), October 1991.

6. Balch, D. T., "Correlation of Full Scale Wind Tunnel Test Data with Model Rotor Data and Theory for a Modern Helicopter Main Rotor," Journal of the American Helicopter Society, Vol. 24, (2), July 1979.

7. Jepson, D., Moffitt, R., Hilzinger, K., and Bissell, J., "Analysis and Correlation of Test Data from an Advance Technology Rotor System," NASA CR-3714, August 1983.

8. Langer, H. J., Peterson, R. L., and Maier, T. H., "An Experimental Evaluation of Wind Tunnel Wall

Correction Methods for Helicopter Performance," American Helicopter Society 52nd Annual Forum, Washington, D.C., June 1996.

9. Tung, C., Bousman, W. G., and Low, S., "A Comparison of Airload Data Between Model-Scale Rotor and Full-Scale Flight Test," American Helicopter Society Aeromechanics and Product Design, October 1995.

10. Bousman, W. G., "A Note on Torsional Dynamic Scaling," Journal of the American Helicopter Society, Vol. 43, (2), April 1998.

11. Torok, M. S., and Goodman, R. K., "Analysis of Rotor Blade Dynamics Using Experimental UH-60A Airloads Obtained at the DNW," Journal of the American Helicopter Society, Vol. 39, (1), January 1994.

12. Rae, W. H., and Pope, A., "Low-Speed Wind Tunnel Testing," 2nd Edition, John Wiley & Sons, New York, 1984.

13. Kufeld, R. M., and Bousman, W. G., "UH-60A Airloads Program Azimuth Reference Correction," Journal of the American Helicopter Society, Vol. 50, (2), April 2005.

14. Keys, C. N., McVeigh, M. A., Dadone, L, and McHugh, F. J., "Estimation of Full-Scale Rotor Performance from Model Rotor Test Data," Journal of the American Helicopter Society, Vol. 30, (4), October 1985.

15. Shinoda, P. M., Yeo. H., and Norman, T. R., "Rotor Performance of a UH-60 Rotor System in the NASA Ames 80- by 120-Foot Wind Tunnel," Journal of the American Helicopter Society, Vol. 49, (4), October 2004.